Journal of Hydrology 555 (2017) 600–620

Contents lists available at ScienceDirect

Journal of Hydrology

journal homepage: www.elsevier.com/locate/jhydrol

Research papers

Review of complex networks application in hydroclimatic extremes with an implementation to characterize spatio-temporal drought propagation in continental USA

Goutam Konapala, Ashok Mishra *

Glenn Department of Civil Engineering, Clemson University, Clemson, SC 29634, USA

ARTICLE INFO

Article history:
Received 3 August 2017
Received in revised form 15 October 2017
Accepted 17 October 2017
Available online 24 October 2017
This manuscript was handled by G. Syme, Editor-in-Chief

Keywords:
Complex networks
Event synchronization
Network theory
Extreme events
Drought

ABSTRACT

The quantification of spatio-temporal hydroclimatic extreme events is a key variable in water resources planning, disaster mitigation, and preparing climate resilient society. However, quantification of these extreme events has always been a great challenge, which is further compounded by climate variability and change. Recently complex network theory was applied in earth science community to investigate spatial connections among hydrologic fluxes (e.g., rainfall and streamflow) in water cycle. However, there are limited applications of complex network theory for investigating hydroclimatic extreme events. This article attempts to provide an overview of complex networks and extreme events, event synchronization method, construction of networks, their statistical significance and the associated network evaluation metrics. For illustration purpose, we apply the complex network approach to study the spatio-temporal evolution of droughts in Continental USA (CONUS). A different drought threshold leads to a new drought event as well as different socio-economic implications. Therefore, it would be interesting to explore the role of thresholds on spatio-temporal evolution of drought through network analysis. In this study, long term (1900–2016) Palmer drought severity index (PDSI) was selected for spatio-temporal drought analysis using three network-based metrics (i.e., strength, direction and distance). The results indicate that the drought events propagate differently at different thresholds associated with initiation of drought events. The direction metrics indicated that onset of mild drought events usually propagate in a more spatially clustered and uniform approach compared to onsets of moderate droughts. The distance metric shows that the drought events propagate for longer distance in western part compared to eastern part of CONUS. We believe that the network-aided metrics utilized in this study can be an important tool in advancing our knowledge on drought propagation as well as other hydroclimatic extreme events. Although the propagation of droughts is investigated using the network approach, however process (physics) based approaches is essential to further understand the dynamics of hydroclimatic extreme events.

1. Introduction

Hydroclimatic extreme event (e.g. floods and droughts) is the result of complex physical processes and is often characterized by multiple climatological and hydrological parameters that vary across a wide range of spatial and temporal scales (Mishra and Singh, 2010). For instance, floods are not only dependent on high precipitation events, but also on the land cover type and water management structures (Peterson et al., 2013). Similarly, droughts too are controlled by multiple climate and human factors making it extremely difficult to determine their important drivers (Mishra and Singh, 2010). In addition to that, these events are detrimental to multiple sectors like infrastructure, human life, water supply, water quality, energy and agriculture (Mishra and Singh, 2010; Rajsekhar et al., 2015). For example, the economic loss of USD 350 billion can be attributed to hydroclimatic extremes (NCEI, 2017) in USA (since 1980 to till date). As a result, it is important to understand the mechanisms of hydroclimatic extreme events, and to build more plausible early warning systems to mitigate these losses (Basher, 2006; Mishra and Singh, 2011; Van loon, 2015).

The evolution of variables triggering hydroclimatic extremes often differs in terms of magnitude, duration and spatial extents. For example, the magnitude of extreme precipitation along with their timing and seasonality are significant drivers of floods,

* Corresponding author.
E-mail address: ashokm@g.clemson.edu (A. Mishra).

https://doi.org/10.1016/j.jhydrol.2017.10.033
0022-1694/

whereas, drought events are triggered by dynamical interaction of atmospheric variables such as precipitation and evapotranspiration over a longer period of time. Therefore, an index that integrates the coevolution of these variables is typically studied to understand droughts. The hydroclimatic extremes are often analyzed using different statistical techniques, such as, frequency estimation (Mckee et al., 1993; Hamed and Rao, 1999; Song and Singh, 2010; Sun et al., 2014), multivariate analysis (Kao and Govindaraju, 2010; Hao et al., 2013; Rajsekhar et al., 2015), wavelet analysis (Jain and Lall, 2001; Kim and Valdés, 2003; Adamowski, 2008; Özger et al., 2009), clustering (Stahl and Demuth, 1999; Bunde et al., 2005; Srinivas et al., 2008; Yang et al., 2013; Rajsekhar et al., 2015) and Bayesian methods (Kuczera, 1999; Kwon et al., 2016; Mishra and Singh, 2009; Madadgar and Moradkhani, 2013). Unlike floods, droughts usually span over large geographical areas and often last for months to years representing a dominant three-dimensional (latitude, longitude and time) space-time drought structure (Lloyd-Hughes, 2012). Therefore, an integrated analysis that factors the spatial behavior into time series analysis are employed to study droughts (Hannaford et al., 2011). As a result, space-time structure of droughts at a regional scale is characterized by studying the severity – area – frequency (SAF) and severity – area – duration (SAD) curves (Mishra and Singh, 2009; Sheffield et al., 2009; Hannaford et al., 2011; Lloyd-Hughes, 2012; Xu et al., 2015; Zhan et al., 2016).

Recent studies have introduced a framework based on network theory to investigate the spatio –temporal characteristics of hydroclimatic extremes (Malik et al., 2012; Boers et al., 2013). A network can be defined as a collection of components (or, units) that are meaningfully connected together. For example, in hydrologic cycle, all the components that are connected to each other can be viewed as a network. Among these components of hydrologic cycle, some components like rainfall and runoff are more strongly connected; whereas, the connections between temperature and groundwater is comparatively weak.

The connection among hydrologic fluxes within the hydrologic cycles varies in terms of their spatio-temporal associations and propagation mechanisms, etc. With this conception, several studies investigated the global linear and nonlinear correlation structure of precipitation and temperature in a networks perspective (Tsonis and Roebber, 2004; Tsonis et al., 2006; Donges et al., 2009a, 2009b; Steinhaeuser et al., 2012; Gozolchiani et al., 2011; Scarsoglio et al., 2013). Several other studies in hydrology have considered smaller, regional networks that focus on a specific variable of interest, like spatial streamflow networks in USA (SivaKumar and Woldemeskel, 2014; Fang et al., 2017), stream flow networks in Canada (Halverson and Fleming, 2015), spatial rainfall networks in Australia (SivaKumar and Woldemeskel, 2015; Jha et al., 2015) and South east Asia (Naufan et al., 2017). These studies surely have advanced our knowledge on the network properties of various climatological variables important to hydrology. However, the advance of complex network approaches application to study the properties of spatio temporal hydroclimatic extremes is still in its nascent stage. Based on the recent developments and applications of complex network theory, it is now possible to advance the quantification of spatio-temporal patterns (evolutions) of hydroclimatologic extreme events using network concepts.

In this regard, this article attempts to introduce the theory and applications of complex network applications for hydroclimatic extreme event to the wider audience of the hydrologic community. This paper provides an overview of complex networks and extreme events, event synchronization method, construction of networks, their statistical significance and the associated network evaluation metrics. We applied network theory concepts and introduced two new metrics specific to the spatio-temporal propagation of droughts in CONUS.

2. An overview of complex networks and their application in characterizing hydroclimate extremes

This section provides an overview of hydroclimatic extremes and different types of relationship between extreme events that can be modeled as networks. A detailed discussion is provided on event synchronization, which was recently applied to quantify the association between extreme events in a number of recent studies. After establishing the background for analyzing extreme events in a network perspective, we discuss different types of networks that can be formed based on the relationships between spatial locations of extreme events. An overview of metrics that were previously used for quantifying the spatio-temporal characteristics of hydroclimatic extreme events from a networks perspective is discussed.

2.1. Identifying hydroclimatic extreme events

The definition of extreme events plays an important in complex network construction. It is necessary to understand the various characterizations of extreme events, before conceptualizing the extreme events that are suitable for network analysis. The extreme events can be selected in multiple ways, however, based on previous studies two distinct methods are commonly used for identification of extreme events (Beniston et al., 2007; Alexander et al., 2006; Groisman et al., 2001; Kharin et al., 2007; Sillmann et al., 2013; Mishra and Singh, 2012; Leonard et al., 2014; Smakhtin, 2001). The first method is based on absolute magnitudes (i.e. highest/lowest value) within a given year. This methodology provides a single value of extreme event per year, which is beneficial for water resources planning and management. However, since this methodology extracts a single extreme event per year, other events that can be an extreme but are lesser/higher in magnitude than highest/lowest event might be neglected. As a result, unless the data length is sufficiently long (>50 years), the complex network might not capture the dynamics of all the extreme events. The second approach is based on threshold values (e.g. >95th and 99th percentiles) to select extreme events. By using this approach it is possible to capture sufficient number of events that can be useful to replicate the characteristics of hydro climatic extreme events in a region. However, the selections of thresholds are rather arbitrary resulting in inaccurate extreme event quantification (Beguería, 2005; Thibaud et al., 2013). Therefore, these limitations should be considered before selecting hydroclimatic extreme events for network analysis.

Previous studies have mainly used the threshold approach to quantify the extreme events. For example, Malik et al. (2012) used threshold approach (i.e. 90th and 94th percentile) for characterizing the extreme precipitation events during the period of 1951–2007. The authors have indicated that the chosen thresholds are useful during the active phase of the Indian Summer Monsoon which is critical to Indian subcontinent. By using these thresholds, they were able to study the spatial structures of underlying atmospheric processes responsible for the active phase of monsoon. Similarly, many studies used the concept of thresholds to study the spatio-temporal characteristics of South American Monsoon (Boers et al., 2013, 2014a,b, 2016; Feldhoff et al., 2015) and Asia (Su-hong et al., 2014; Stolbova et al., 2014). Similarly a recent study (Rheinwalt et al., 2016) adopted complex networks to study the spatio-temporal characteristics of extreme rainfall in Germany using magnitude based thresholds (i.e. daily rainfall >10 mm).

Therefore, depending on the objective and data availability, appropriate threshold needs to be selected to generate sufficient number of extreme events for constructing complex networks of extreme events.

2.2. Relationship between hydroclimate extremes

Once the extreme events are defined, the next step is to identify the type of relationship between extreme events. Generally, relationships between any two variables can be broadly characterized into the two categories, i.e. causal and functional connectivity (Wright, 1921). A causal relationship indicates that one event is the result of occurrence of another event. For example, occurrence of rainfall is one of the primary reasons for streamflow generation. Hence, this type of relationship could be categorized as causal. Previous studies, particularly with respect to climate networks have analyzed these causal relationships between variables using linear approach of Granger Causality (Granger, 1969) and a nonlinear approach of transfer entropy (Schreiber, 2000). Recently, using causal networks, Ebert-Uphoff and Deng (2012)have identified the causal relationship among the four prominent modes of atmospheric low-frequency variability in boreal winter including the Western Pacific Oscillation (WPO), Eastern Pacific Oscillation (EPO), Pacific–North America (PNA) pattern, and North Atlantic Oscillation (NAO). Mokhov et al. (2011) used Granger causality to identify the mutual influence between El-Nino/ Southern Oscillation and atmospheric processes in Europe. In another related study, Runge et al. (2015) identified causal pathways to gain insights into the Pacific–Indian Ocean interactions and Indian Summer monsoon. However, these networks have not been applied until now to identify the causal relationships associated with extreme events. Therefore, in this article we did not focus on building networks based on causal relationships.

Functional connectivity is another type of relationship, which indicates that two variables vary in a synchronized manner and coevolve together. For instance, the coevolution of droughts between two distinct locations may have similar spatio- temporal patterns, but they may not have causal relationship. However, it can be hypothesized that the atmospheric mechanisms triggering these droughts might be similar (Rajsekhar et al., 2012; Mishra et al., 2015). This kind of relationship was previously applied in hydroclimatic studies such as prediction of variables in ungauged river basins (Sivapalan, 2003; Samaniego et al., 2010), and drought regionalization (Portela et al., 2015; Yoo et al., 2012), etc. A key advantage of applying complex network theory in this context is that it does not require additional climate variables and indices to analyze spatiotemporal patterns (Malik et al., 2012). In this article, we focused on analyzing spatio-temporal patterns of hydroclimatic extremes using functional connectivity type of relationship to develop complex networks.

Pearson's correlation coefficient is a popular metric to quantify the linear dependence between any two variables (Hlinka et al., 2014). However, Pearson correlation coefficient assumes that the variables follow a Gaussian distribution (Von Storch, 1999). Therefore application of Pearson correlation coefficient in case of variables that follow non-Gaussian distributions may be suboptimal and it may not capture the complex dependence between extreme variables. In addition, evolutions of hydroclimatic extreme events are non-uniformly distributed over time creating irregularly spaced data series. Analysis of event-based time series can be challenging using similarity measures like Pearson's correlation might not perform well in these contexts. Extremogram (Davis and Mikosch, 2009), copulas (Gudendorf and Segers, 2010) and rearrangement functions (Puccetti and Wang, 2015), and event synchronization (Quiroga et al., 2002) can be applied to quantify the functional relationship between extreme events. Among them, the event synchronization technique was recently applied in complex network analysis, which is discussed in the next section.

2.2.1. Event synchronization (ES) methodology for determining association between extreme events

Malik et al. (2012) applied Event synchronization (ES) methodology for finding the relationship between extreme events occurring at different spatial locations. Event synchronization counts the number of temporally coinciding events in any two-event series by allowing small deviations between the occurrences of the events, i.e., a dynamical delay between the events occurring at two different spatial units (i.e., climatic locations). As a result, this metric does not assume any probability distribution to be followed by the underlying data. In addition to that, as it explicitly considers the only coincidence of extreme events between two regions excluding the remaining time period, it is precisely suitable for irregularly spaced data like the extreme events.

Once the extreme events are extracted, in order to decide if two events at locations l and m are synchronous, we first estimate the dynamic delay is estimated as

$$\tau_{lm}^{ij} = \min \frac{\{t_l^i - t_l^{i-1}, t_l^{i+1} - t_l^i, t_m^i - t_m^{i-1}, t_m^{i+1} - t_m^i\}}{2} \tag{1}$$

In this context, t_l^i represent the time index when the extreme event i has occurred in the region l. Similarly, t_m^j would represent the time index when the extreme event j has occurred in region m. The difference $t_l^i - t_l^{i-1}$ indicates waiting time between two consecutive extreme events in location l. The same interpretation can be extended for other regions and events. To exclude unreasonable long dynamic delays, a maximum delay of τ_{max} is selected between the extreme events occurring at two locations. Now, if $0 < d_{lm}^{ij} < \tau_{lm}^{ij}$ and $0 < d_{lm}^{ij} < \tau_{\max}$, then events i and j at location l and m are considered as synchronous events with the event at l preceding event at m.

Mathematically, it can be expressed as

$$S_{lm}^{ij} = \begin{cases} 1 & \text{if } 0 < d_{lm}^{ij} < \tau_{lm}^{ij} \text{ and } 0 < d_{lm}^{ij} < \tau_{\max} \\ 0 & \text{otherwise} \end{cases} \tag{2}$$

Now, ES_{lm} can be estimated as the relative number of extreme events at l occurring before events at m as

$$ES_{lm} = \frac{\sum_{ij} S_{lm}^{ij}}{n_l} \tag{3}$$

where n_l represents the total number of events at location l. Similarly, the relative number of extreme events at m occurring before events at l is estimated as

$$ES_{ml} = \frac{\sum_{ij} S_{ml}^{ij}}{n_m} \tag{4}$$

where n_m represents the total number of events at location m. This procedure is performed for all combinations of locations N with where extreme events can be measured to derive a matrix of ES values with the dimension of $N \times N$. It is important to notice that, the ES matrix is not symmetric in nature. For instance, the value ES_{ml} represents how likely an extreme event in location m can propagate to location l, which is different from the value of ES_{ml}. Therefore, each element in the ES matrix represents the likelihood of extreme event propagation from one location to the other regions.

2.2.2. Estimating statistically significant event synchronization (ES) values

One way to extract statistically significant values is by utilizing the bootstrapping method (Efron and Tibishirani, 1999). In this methodology, for estimating statistical significance, 1000 surrogate pairs of event time series with n_l events at location l and n_m events at location m placed independently as a uniformly random distribution of extreme events. Then the ES metric is calculated for all the possible pairs. In this way, 1000 values of event synchronization metrics for each pair of nodes is obtained. Now depending on the desired significance level (i.e. 0.1, 0.05, 0.01), the corresponding percentile (i.e. 90th, 95th and 99th) of these 1000 null models is estimated as ES^T. By using actual number of extreme events at locations l and m, the original distribution of events was preserved as suggested by Boers et al. (2013, 2014a). For an ES value to be statistically significant at the desired significance level, it should be greater than ES^T value.

2.3. Representation of hydroclimate extremes as networks

In purely mathematical sense, a network or graph can be defined as a group of nodes or vertices that are connected together. The connections between any two nodes are called as links or edges. When analyzing the spatio-temporal extreme events, studies until now have considered the spatial locations of extreme event occurrence as nodes, whereas the relationship between two nodes with respect to the extreme events (i.e. ES value) as links. Typically, a network can be illustrated in pictorial as a set of nodes joined by lines for the edges. A network can be stored as a two dimensional matrix ($N \times N$) commonly known as adjacency matrix, where N is the total number of nodes in a network. In the matrix, each element represents the presence/absence of an edge between any two nodes. By changing the edge types, we can possibly construct four types of networks (Figs. 1a, c and 2a, c). Similarly the adjacency matrix will change depending on the network type (Figs. 1b, d and 2b, d). In the following text, we discuss the differences between each network type and their corresponding adjacency matrices.

Fig. 1(a) represents the simplest form of network where the presence of links between nodes is represented without any perception of direction or weight. Therefore, the presence/absence of links in a network between nodes can be represented as binary values. We illustrate this in Fig. 1(b), where the presence of link between two nodes is represented as a black dot in the matrix whereas; if there is no entry it corresponds to no links. We can observe that the corresponding adjacency matrix of an unweighted-undirected matrix is symmetric in nature. Fig. 1(c) represents the presence of links between nodes with their respective weights. These weights distinguish one link from another. Therefore, correspondingly, the adjacency matrix also changes as shown in Fig. 1(d). Instead of the dark dots in the matrix, we see the colored dots scaled to weights of the links. However, it is important to note that the matrix is still symmetric. Therefore, for undirected networks, the adjacency matrix is symmetric; however, the presence/absence of weights might change the element structure in the adjacency matrix. These kind of networks have been previously employed to primarily understand the atmospheric process causing the extreme events (Malik et al., 2012; Boers et al., 2013, 2014a,b, 2015a,b, 2016; Feldhoff et al., 2015).

In addition to the above two networks, we can also represent direction/flow between the nodes in a network. Fig. 2(a) represents a network of nodes with edges that have a direction. Once the direction is introduced, the two way relationship does not hold true. For example, in the Fig. 2(a), we can see that node *a* has a link directed towards *e*, but not the opposite. As a result, the same is reflected in the adjacency making it asymmetric (Fig. 2b). However, since there are no weights assigned to the network, it still is binary in nature. Fig. 2(c) and (d) represent the weighted version of directed network and its corresponding adjacency matrix. By using networks where direction can be included, we can construct network that can possibly represent the spatio-temporal propagation of the extreme events. This propagation concept was explored in studies by Boers et al. (2015a,b) and Marwan and Kurths (2015) to develop a prediction scheme of extreme rainfall events pertaining to South American monsoons. Therefore, depending on the goal of the study, we should carefully select the type of network to be utilized. Other more advanced and complicated networks like multiplex networks, interdependent networks where a group of networks interact with each other forming a network of networks are also possible. However, for this study we focus on the above four network types.

2.4. Network metrics

We discuss some basic network metrics that have been used in studying the hydroclimatic extreme events. In addition to that, we also indicate how these studies have interpreted these metrics with respect to the characterization of extreme events.

2.4.1. Degree and its probability distribution

Degree is one of the most intuitive and basic measure of a complex network. Degree measures the total number of connections from a particular location l to all the other N locations (Fig. 3). In case of undirected-unweighted adjacency matrix A, it can be expressed as shown in Eq. (5).

$$D_l = \sum_{m=1}^{N} A_{lm} \tag{5}$$

where N represents the total number of nodes in a network. Therefore, when using ES methodology, if the extreme events at a particular location is in sync with extreme events occurring at relatively more number of locations, then it is said to have higher degree values. Determining the probability distribution of degrees in a network is another measure that gives insight on the structural properties of a network. For example, if the degree distribution follows a binomial distribution, it could be termed as a random network, where each node is connected with an independent probability (Erdos and Rényi, 1960). Whereas, if the degree distribution follows a power law form, then those networks are more real world-like and the nodes are connected in a preferential way (Albert and Barabási, 2002). However, it was found that usually this type of power law behavior is found only in sparsely connected networks. Nevertheless, denser networks exhibit a divergence of power law behavior (Callaway et al., 2000).

Malik et al. (2012) analyzed annual extreme rainfall events in Indian summer monsoon, and observed that high degrees are observed in northwest Pakistan and lowest values occur in southeast India. The authors suggested that the high degree values are mainly due to longer spatial connections of Indian summer monsoon extremes in these regions. In addition to that, a bimodal Poisson probability distribution was observed revealing the two modes of Indian summer monsoon rainfall extremes. Similarly, Stolbova et al. (2014) calculated the degree metric separately based on the pre-monsoon, monsoon and post monsoon for the Indian Subcontinent and observed that the spatial distribution of high degree regions are not similar indicating a possibility of different rainfall extreme mechanisms among the seasons. In case of South American Monsoon system, Boers et al. (2013) indicated that high degree values for extreme rainfall event were found in regions of northeastern Brazil to Amazon basin and along the eastern slopes of the central Andes and the adjacent subtropical Atlantic Ocean. This

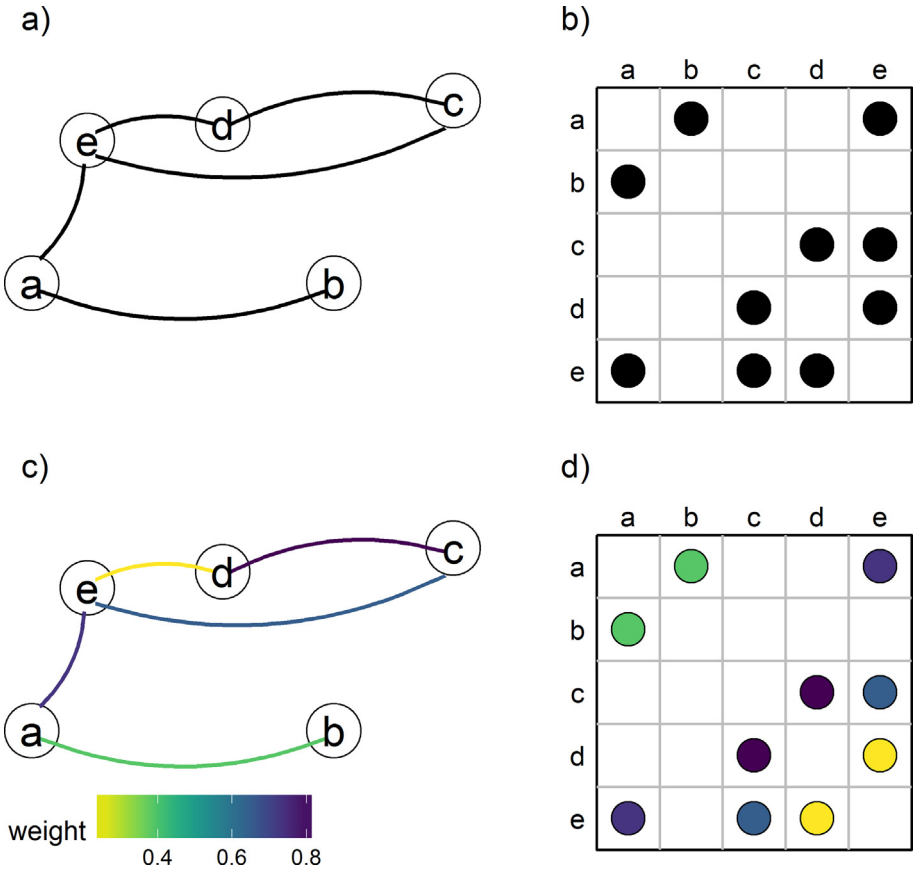

Fig. 1. A simple schematic representation of (a) undirected-unweighted network and its corresponding (b) adjacency Matrix layout. Similarly, we also illustrate (c) the undirected-weighted network and its corresponding (d) adjacency matrix's layout. The black dots in (b) represents the presences of links between the nodes in (a). Similarly, the colored dots represents the weighted links between nodes in the network shown in (c). (For interpretation of the references to colour in this figure legend, the reader is referred to the web version of this article.)

spatial pattern indicates the main and well-known climatological moisture pathways along which extreme rainfall events synchronize (Vera et al. 2006; Marengo et al. 2012).

2.4.2. Regional connectivity

This degree metric is further modified to represent local connectivities of certain region R that have been known to be particularly important for extreme events occurrence. The regional connectivity (*RC*) of a location *i* to a comparatively larger region *R* is defined as the number of links connecting *i* and any location within that region. It can be expressed as

$$RC_l(R) = \sum_{m \in R} A_{lm} \tag{6}$$

This measure can thus be used to assess the spatial locations where extreme events occur synchronously with events in a given region *R* under consideration. For example, Boers et al. (2015a,b) used this metric to compare how the rainfall extreme events of regions important to south American monsoon system are connected in various available datasets. The authors have identified some significant differences in regional connectivity for the study regions among the selected datasets. In an another article (Boers et al., 2016), utilized the *RC* to identify the regional connectivity of Altiplano and Puna Plateaus along with four mountainous catchments in Andes Region belonging to South America for different classifications of extreme rainfall events. Through this metric it was observed that the extreme rainfall events originating in Andes have spatially distant connections in South America indicating the influence of rossby wave activity (Hoskins and Ambrizzi, 1993) as well as several frontal systems (Salio et al. 2007; Romatschke and Houze, 2010).

2.4.3. Strength and network divergence

Even though, degree metric was useful in detecting various spatio-temporal characteristics of extreme rainfall events, it does not consider the direction and weightage of the connections. As mentioned before, the inclusion of weight and direction of the connections might improve the representation of extreme event propagation. This weighted and directed version of degree is known as strength. To clearly explain the strength metric, we refer to Fig. 4, which illustrates two hypothetical scenarios, where the location *l* is connected to other locations with varying intensity of ES value. For example, if an extreme event starts in location *l*, then most likely it propagates to region *m* since its ES value is highest among the others (Fig. 4a) and it is less likely to propagate to region *t* due to its low ES value. Therefore, it is obvious that the sum of all the ES values originating from location *l* will indicate the resultant influence of the location *l* in propagating extreme events to other locations. As a result, *outward-strength* given by Eq. (7).

$$Sr_l^{out} = \sum_{m=1}^{N} C_{lm} \tag{7}$$

where *N* is the total number of nodes present in a network and *C* represents the adjacency matrix which is both weighted and directed. Therefore, higher the magnitude of Sr_l^{out}, the higher is the influence of the location *l* in extreme event propagation. Similarly,

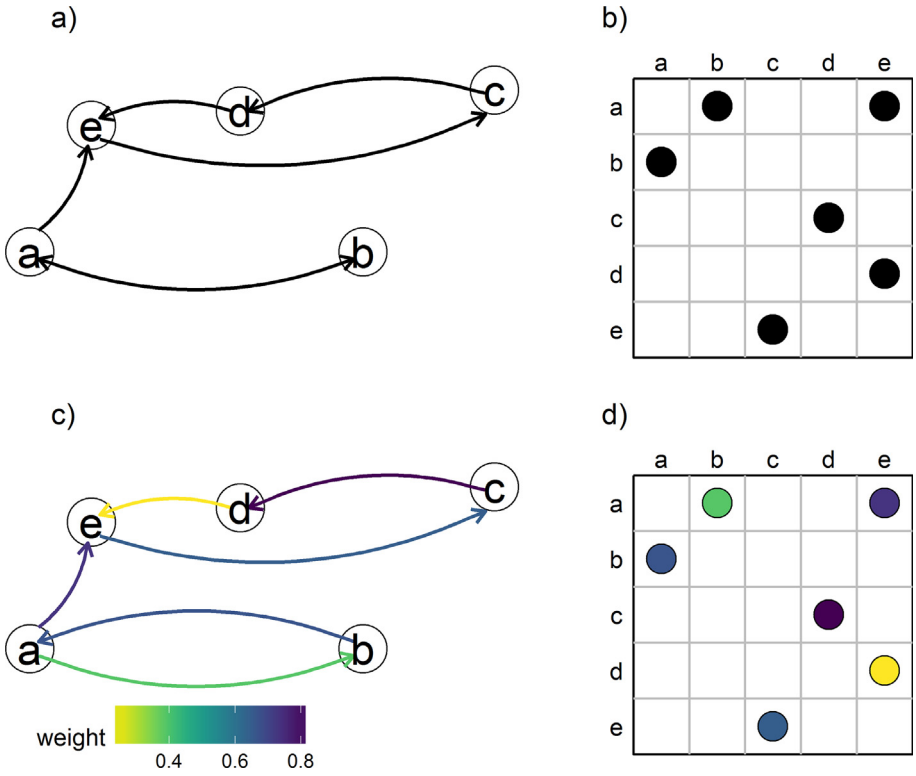

Fig. 2. A simple schematic representation of (a) directed-unweighted network and its corresponding (b) adjacency Matrix layout. Similarly, we also illustrate (c) the directed-weighted network and its corresponding (d) adjacency matrix's layout. The black dots in (b) represents the presences of links between the nodes in (a). Similarly, the colored dots represents the weighted links between nodes in the network shown in (c). (For interpretation of the references to colour in this figure legend, the reader is referred to the web version of this article.)

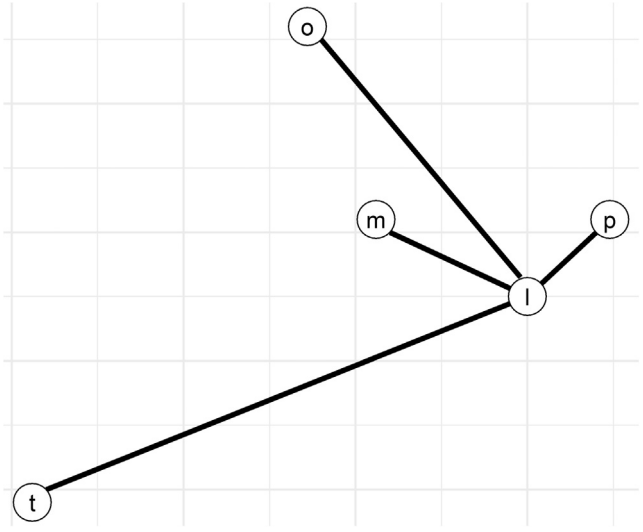

Fig. 3. A simple schematic representation of degree. The alphabets (l, m, o, p and t) depict the nodes and the lines depict the presence of network connections.

(Fig. 4b) represents that if an extreme event starts in location *o*, then most likely it would propagate to location *l* due to its high ES value. Whereas, it is less likely that an event from region *t* can propagate to *l* because of its low ES value. The sum of ES values directed towards location *l* will indicate the vulnerability of region *l* to events happening elsewhere. This sum of ES values better known as *inward-strength* is given by Eq. (8).

$$Sr_l^{in} = \sum_{m=1}^{N} C_{ml} \tag{8}$$

where *N* is the total number of nodes present in a network. Therefore, higher the Sr_l^{in}, higher will be the vulnerability of a climate division to spatial propagation of the extreme events. Utilizing these two definitions, a new measure called as network divergence defined as the difference of in-strength and out-strength at each location is calculated as shown in Eq. (9)

$$\Delta Sr_l = Sr_l^{in} - Sr_l^{out} \tag{9}$$

Positive values of *DS* indicate sinks of the network: extreme events in these spatial locations are preceded by extreme events in other locations. For example, a region with a high positive value of *DS* would indicate that it is more likely for the extreme events to start at that particular location and subsequently propagate to other locations. Whereas, negative values indicate sources: extreme events in these locations are followed after extreme events in other locations. Regions with high negative values of *DS* as thus considered as spatial sinks of extreme events. Similarly, a weighted and directed regional connectivity of a region can also be defined as

$$RC_l^{out}(R) = \frac{1}{|R|}\sum_{m\in R} C_{lm} \tag{10}$$

$$RC_l^{in}(R) = \frac{1}{|R|}\sum_{m\in R} C_{ml} \tag{11}$$

where |R| denotes the number of locations contained in region *R*. Using these definitions, Boers et al. (2015a,b) developed a prediction scheme with an accuracy of 60%, which increases to 90% during El Nino conditions of extreme rainfall events in Eastern Central Andes region of South America.

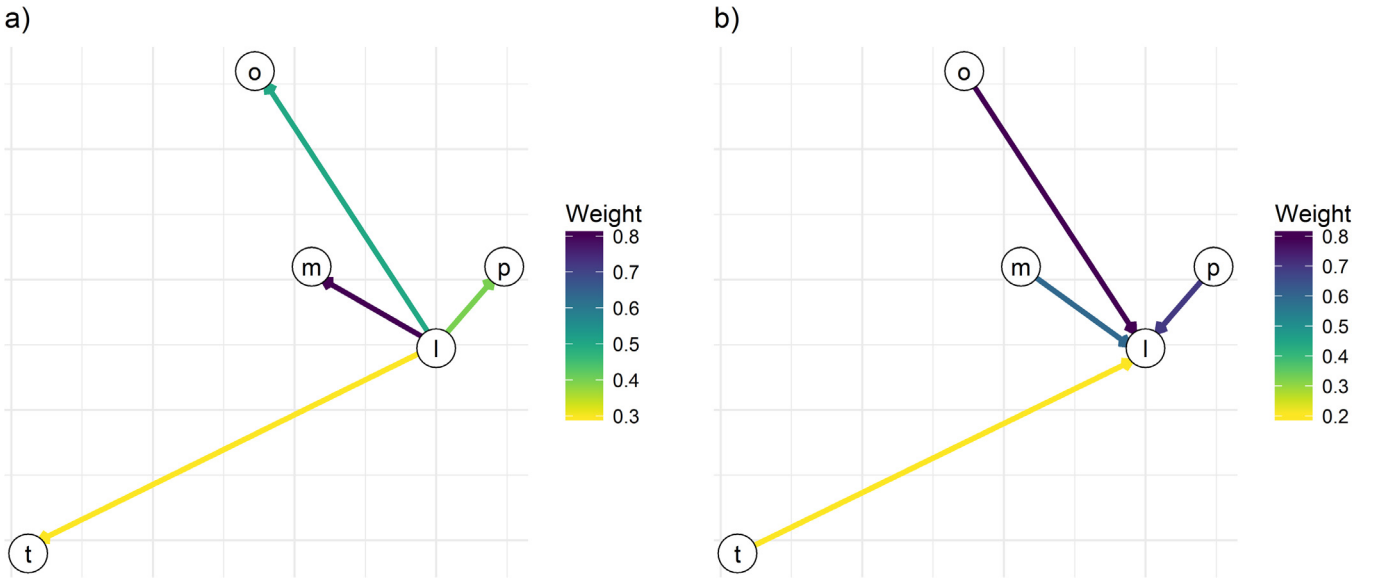

Fig. 4. A simple schematic representation of (a) outward-strength, and (b) inward-strength. In both the cases, the alphabets (l, m, o, p and t) depicts the nodes. The colored arrows illustrate the weight of the links between the nodes. The direction of arrows represent the direction of event propagation. (For interpretation of the references to colour in this figure legend, the reader is referred to the web version of this article.)

2.4.4. Local and global clustering coefficient

Clustering coefficient quantifies one of the fundamental properties of a network, which measures the extent to which nodes tend to cluster in a network (Watts and Strogatz, 1998). More particularly, the local clustering coefficient and global clustering coefficient are recently utilized to the study the characteristics of Indian and South American monsoon systems. As the name suggests, the local clustering coefficient is computed at the node level, whereas, global clustering coefficient is computed for the whole network. The local clustering coefficient of location i measure the probability that two randomly chosen connections of l are also connected. For an unweighted-undirected network it can be calculated as the ratio of number of triangles connected to a location l and the total number of possible pairs given by Eq. (12)

$$LCC_l = \frac{\sum_{k<m} A_{lm}.A_{kl}.A_{km}}{\sum_{k<m} A_{lm}.A_{kl}} \tag{12}$$

where l, m, k represent any three nodes in a network and A represents its adjacency matrix. The global clustering coefficient (Watts and Strogatz, 1998) is calculated based on the average local clustering coefficients of all the nodes in a network, as shown in Eq. (13).

$$GCC = \sum_{i=1}^{N} \frac{LCC_i}{N} \tag{13}$$

where, N represents the total number of nodes present in a network.

Regions with higher local clustering coefficient (LCC) indicate a spatially homogeneous phenomenon, whereas, global clustering coefficient (GCC) gives the overall cohesiveness of a network. Malik et al. (2012) and Boers et al. (2013) have indicated that the lower values of the LCC can be related with more fragmented extreme rainfall fields, whereas larger values represent a more clustered activity in the case of Indian Summer and South American Monsoon, respectively. The GCC was used to study the co-evolution of South American monsoon extreme event and its associated moisture divergence network with ENSO index (Boers et al., 2015a,b). It was observed that GCC of extreme event networks related to moisture divergence are negatively correlated with ENSO index, whereas the extreme precipitation event networks do not show any significant correlation. (Boers et al., 2015a,b)

2.4.5. Betweenness centrality

Betweenness centrality is a path based metric based on the shortest paths between two nodes. Betweenness centrality is a prominent metric for information transfer, which suggests that nodes with higher betweenness centrality have more information passed through them than the other nodes. Mathematically, it is given by

$$BC_l = \frac{\sum_{k\neq l\neq m} \sigma_{km}(l)}{\sum_{k\neq l\neq m} \sigma_{km}} \tag{14}$$

where $\sum_{k\neq l\neq m} \sigma_{km}$ is the total number of shortest paths between k and m and $\sum_{k\neq l\neq m} \sigma_{km}(l)$ indicates the same but passing through location l. In general, it was found that nodes with high betweenness centrality have more information passed through them than the other nodes. Therefore, in the context of extreme rainfall events too, Malik et al. (2012) and Boers et al. (2013) hypothesized that the regions with high betweenness are important information pathways for extreme rainfall events. However, even though the clustering coefficient and betweenenss centrality metrics have been applied to characterize spatio-temporal characteristics of extreme events, the studies often lack solid physical basis for the observed spatial variations.

3. Application of complex network approach to study the spatio-temporal propagation of drought in continental USA

To illustrate the usefulness of the above presented networks approach, we study the spatio-temporal propagation of droughts in CONUS. The spatio-temporal evolution of drought is a complex process as the hydro-climatic processes are inter-connected at different spatial units (i.e., local to regional scale) (Mishra and Singh, 2010). Considering that drought has larger spatial and temporal extent, the application of complex networks can be a useful tool to study the propagation of drought. In addition to that, no prior study investigated the spatio-temporal characteristics of drought events in CONUS from the perspective of networks based on event

synchronization. Therefore, in this section, a network approach based on the event synchronization is applied to investigate the dynamic synchronization properties of droughts in continental CONUS by including their spatiotemporal characteristics for the period of 1900–2016. We utilize the network metrics related to weighted-directed network for studying the spatio-temporal propagation of droughts in CONUS. In addition to that, we also introduce two metrics that quantify the dominant orientation and distance travelled by droughts in the following example application.

3.1. Drought data description and source

Palmer Drought Severity Index (PDSI) is one of the commonly used indicators for monitoring droughts (Mishra and Singh, 2010). Several studies used PDSI to investigate the spatial and temporal drought characteristics (Mishra and Singh, 2010; Karl and Koscielny, 1982). We used monthly PDSI time series available for 344 climatic divisions of CONUS during the period of 1900–2016, which was obtained from the United States climatic divisional database available through the National Oceanic and Atmospheric Administration.

PDSI is derived based on the principles of moisture supply and demand utilizing the precipitation and temperature variables of a region. The data for the climate divisions have been corrected for time-of observation bias (Karl et al., 1986). It was found that even in the regions of complex terrain, such as the mountainous areas of the western U.S., the standardized departures of temperature and precipitation from normal are spatially consistent within a climate division (Karl and Riebsame, 1984). The presence of these attributes motivated us to use PDSI climate division data sets in our study.

3.2. Selection of drought event threshold

The PDSI was used to quantify the conditions of water surplus as well as deficit at any given location. Positive and negative values of PDSI usually represent wet and dry conditions of a region, respectively. Therefore, drought event (e.g., mild to extreme) can be categorized based on negative thresholds of the PDSI time series. Also, different threshold leads to a new drought event as well as different socio-economic implications. For example, human health risks, water quality concerns and plant stresses are found to be markedly different for mild (PDSI < -1) and moderate droughts (PDSI < -2) (Mishra and Singh, 2010). Therefore, it would be interesting to explore the role of thresholds on spatio-temporal evolution of drought through network analysis. In addition to that, as we use drought onset time for constructing the networks, it will be relevant to study the potential influence of 'threshold' on the spatio-temporal drought propagation characteristics at different severity levels. Hence, we classify the onset of drought events using two types of threshold: (a) Mild drought onset based on PDSI < -1 with duration ≥ 3 months, and (b) Moderate drought onset based on PDSI < -2 with duration ≥ 3 months. It is important to note that our threshold definition is more focused towards initiation of mild and moderate drought events. We did not focus on initiation of extreme droughts as it will reduce the number of events in our analysis. By using longer drought periods, we only consider the sizeable events and distinguish them from smaller duration events that might not pose significant risks.

3.3. Event synchronization (ES) methodology for drought event analysis

The temporal distributions of drought events are typically non-uniformly distributed, which is appropriate for ES application. Therefore, we employed ES methodology as explained in Section 2.2.1 to analyze drought events in this study. As explained before, we extracted PDSI time series which has a sequence of mild (moderate) drought events corresponding to months with PDSI < -1 (PDSI < -2) with duration ≥ 3 months for each climate division in CONUS. We introduce a maximum delay of $\tau_{max} = 3$ months between the drought events occurring at two climate divisions. Fig. 5 illustrates a hypothetical example of drought event series between two location l and m. The figure shows that the events within the prescribed time window are considered as synchronized events. It is to be noted that drought events, which occur at the very same time step at different locations, are discarded, since the temporal ordering of events is not determined in those instances. In addition to that, since we utilized the drought onset month for the formulation of ES metric, the value of ES_{lm} qualitatively represents how likely a drought in division l can propagate to division m. Hence, greater the value of ES_{lm}, more likely a drought in l will propagate to m. This procedure is performed for all combinations of climate divisions (l and m), to derive a matrix of ES values with the dimension of 344×344.

3.4. Construction of drought networks

This study aims to characterize the propagation of droughts based on directions with strong spatial preferences using a directed weighted network. Therefore, for preserving only the statistically significant relationships, we use the bootstrapping approach as explained in the Section 2.2.2. We obtain 1000 surrogate values of event synchronization metrics for each pair of climatic divisions and define 99th percentile values of these 1000 null models as ES^T. Using this information, a directed and weighted network link from climate division l to m can be constructed, if ES_{lm} is greater than threshold value of ES^T_{lm} as

$$C_{lm} = \begin{cases} ES_{lm,l\neq m} & \text{if } ES_{lm} > ES^T_{lm} \\ 0, & \text{otherwise} \end{cases} \quad (15)$$

From a network perspective, the resulting matrix C will represent a weighted-directed adjacency matrix of dimension 344×344; where a non-zero element in matrix represents the likelihood of propagation of drought between any two divisions, where each climate division would represent a node.

3.5. Network analysis of drought events

For analyzing the drought networks, we employ the network metric of strength, and introduce two new measures based on strength to characterize the dominant orientation and propagation distance of the droughts. As the strength metric is already defined earlier (Section 2.4.3), we only discuss the contextual meaning of strength in the propagation of drought in this section. However, for other two metrics, we first build the background in the context of drought events and subsequently define them mathematically for illustration purpose.

The magnitude of Sr^{out} [Refer Eq. (7)], can be interpreted synonymous with the influence of the climate division in drought propagation. Higher its magnitude, higher is the influence of the climate division in drought propagation. Similarly, the magnitude of Sr^{in} [Refer Eq. (8)], will indicate the degree of vulnerability of climate division to drought events happening elsewhere. Therefore, higher the Sr^{in}_l, higher will be the vulnerability of a location to spatial propagation of the drought events. In addition to these metrics, we also compute the probability distribution of Sr^{out} and Sr^{in} to study the structural properties of the drought networks in CONUS.

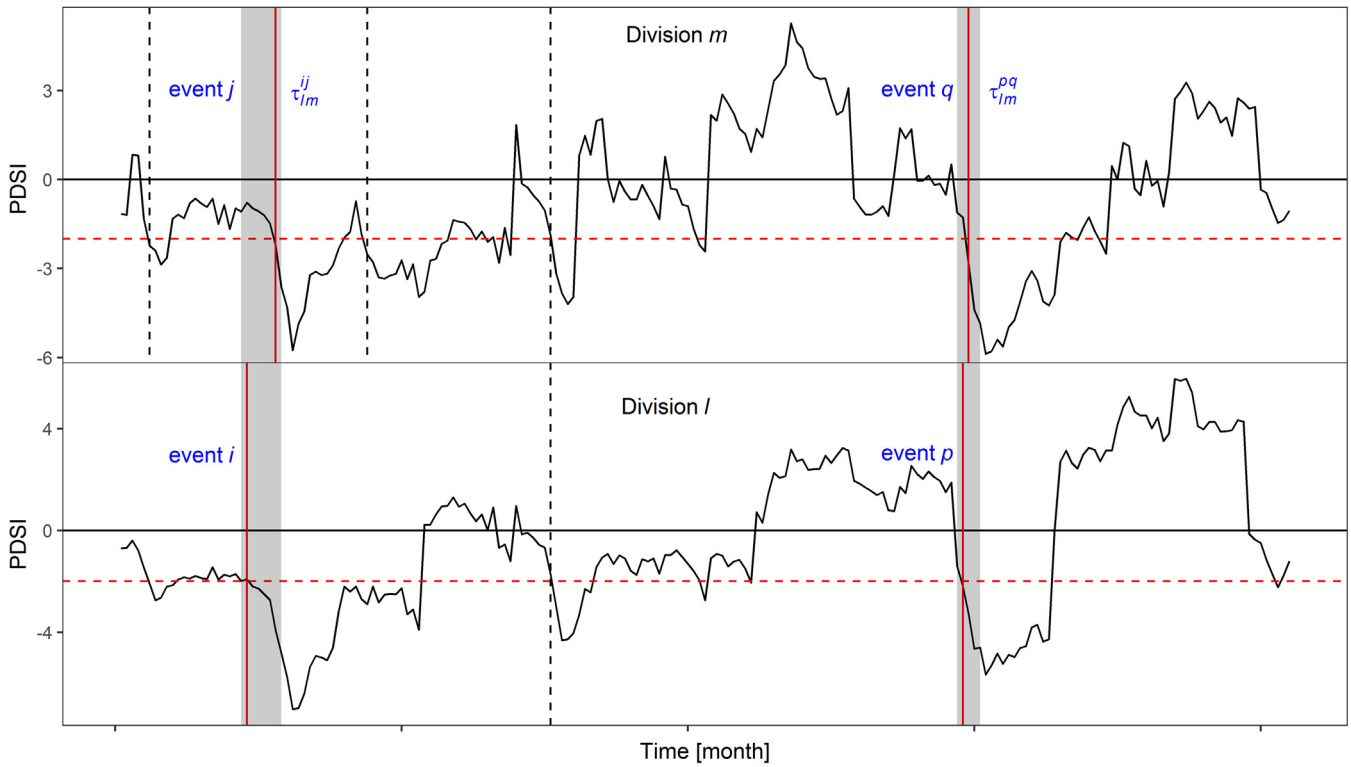

Fig. 5. A hypothetical representation of synchronized onset of moderate drought events. Here, we define the onset of a moderate drought event (vertical red and dotted black lines) as the month when PDSI becomes lesser than −2 (horizontal dashed red line). Drought events (i, p) at climatic division l are said to be synchronized (vertical red lines) with drought events (j, q) at climatic division m, if they occur within the prescribed time window of τ_{lm}^{ij} and τ_{lm}^{pq}, respectively. The events that occur at the very same time step in divisions l and m, are discarded, since the temporal ordering of events is not determined in those instances. (For interpretation of the references to colour in this figure legend, the reader is referred to the web version of this article.)

Now that we have established a framework to assess the critical regions in drought propagation, we further investigated the dominant orientation and geographical distance through which the propagation 'from' and 'to' climate divisions may occur. For the purpose, we introduced the angle (θ_{lm}) between the reference latitude (horizontal line) going through the centroid of division l and the straight-line between the centroids of region's l and m as illustrated in Fig. 6(a); whereas, the length between the centroids of l and m is estimated as geographical distance (D_{lm}). Likewise, we estimated the angle and distance between the climate divisions only if there exists a connection between them (i.e. $C_{lm} > 0$). In the next step, we develop a matrix which contains angles (θ) and distances (D) similar to the matrix C as shown in Eqs. (16) and (17)

$$An_{lm} = \begin{cases} \theta_{lm}, & \text{if } C_{lm} \neq 0 \\ \text{undefined}, & \text{otherwise} \end{cases} \tag{16}$$

$$Di_{lm} = \begin{cases} D_{lm}, & \text{if } C_{lm} \neq 0 \\ \text{undefined}, & \text{otherwise} \end{cases} \tag{17}$$

It is imperative that the calculated angles lie in the range of [0, 2π]; we simplify the directional interpretations by classifying the angle range into eight orientations each of $\pi/4$ and grouping the angles as orientations according to the table 1. As a result, we interpret the directionality as an orientation rather than an angle for simplicity.

Similar to the case of strength, we can estimate the dominant orientations for the links directed towards the selected node (i.e. inward-orientation) as well as links directed from the selected node towards the other nodes (i.e. outward-orientation). Fig. 6 (b) and (c) illustrates the estimation of both out-orientation and in-orientation in a pictorial form for a hypothetical location l. In the case of outward-orientation, initially the out-strength of location l along the predefined orientations can be estimated as shown in Eq. (18)

$$Sr_l^{out}(\phi) = \sum_{m \in \phi} C_{lm} \tag{18}$$

Then the orientation along which outward-strength is maximum can be considered as dominant orientation along which the droughts may propagate. Therefore, we define *outward-orientation* as the principal direction in which droughts may propagate as expressed in Eq. (19).

$$Or_l^{out} = \arg\max_{\phi}(Sr_l^{out}(\phi)) \tag{19}$$

Now, we define its corresponding *outward-distance* as the average geographical distance between the location l and the regions along the outward-orientation as Eq. (20)

$$Dr_l^{out} = \frac{\sum_{m \in Or_l^{out}} Di_{lm}}{n_{Or_l^{out}}} \tag{20}$$

whereas, $n_{Or_l^{out}}$ represents the number of Di_{lm} elements along the orientation Or_l^{out}. As evident from the formulation, Or_l^{out} represents the dominant orientation in which drought at climate division l may propagate. The corresponding Dr_l^{out} indicates the mean geographical distance a drought event in climate division l may propagate along the orientationOr_l^{out}. In the same way, the *inward-strength* of location l along the predefined orientations can be estimated as shown in Eq. (21)

$$Sr_l^{in}(\phi) = \sum_{m \in \phi} C_{ml} \tag{21}$$

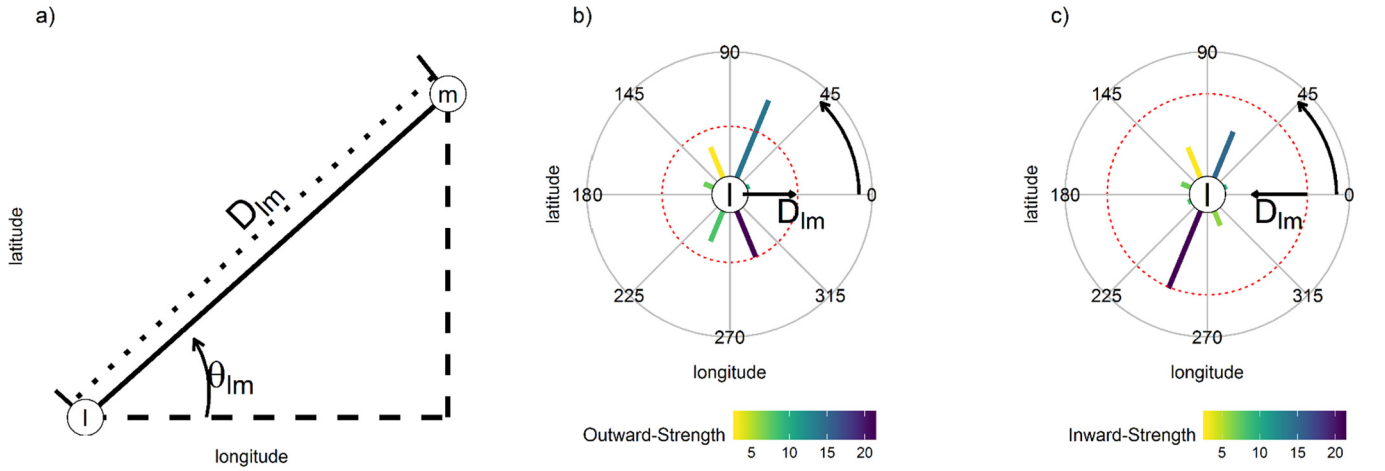

Fig. 6. A schematic representation to aid the calculation of (a) angle and direction. The distance between l and m is the straight line connecting these two centroids. Whereas the direction of propagation is estimated as the angle between the horizontal dotted line and the straight-line connecting climate divisions *l* and *m*. A schematic representation for estimating: (b) outward-orientation, and (c) inward-orientation. In both the cases, the color of the lines illustrates the outward-strength and inward-strength values. The orientation with maximum value of outward-strength and inward-strength is considered as dominant direction for drought propagation. The red dotted line represents the average geographical distance of the dominant outward- and inward-orientation as outward-distance and inward-distance, respectively. (For interpretation of the references to colour in this figure legend, the reader is referred to the web version of this article.)

Table 1
Classification of angles and their corresponding orientation.

Angle (θ)	Orientation (ϕ)
$0 \leq \theta < 45$	East North East (ENE)
$45 \leq \theta < 90$	North North East (NNE)
$90 \leq \theta < 135$	North North West (NNW)
$135 \leq \theta < 180$	West North West (WNW)
$180 \leq \theta < 225$	West South West (WSW)
$225 \leq \theta < 270$	South South West (SSW)
$270 \leq \theta < 315$	South South East (SSE)
$315 \leq \theta < 360$	East South East (ESE)

The orientation along which inward-strength is maximum can be considered as dominant orientation though which drought may propagate to location *l* as expressed in Eq. (22).

$$Or_l^{in} = \arg\max_{\phi}(Sr_l^{in}(\phi)) \tag{22}$$

The corresponding *inward-distance* is estimated as the average geographical distance between the location *l* and the regions along the inward-orientation as shown in Eq. (23)

$$Dr_l^{in} = \frac{\sum_{m \in Or_l^{in}} Di_{ml}}{n_{Or_l^{in}}} \tag{23}$$

where, $N_{Or_l^{in}}$ represents the number of defined Di_{ml} elements along the orientation Or_l^{in} and Or_l^{out} represents the dominant orientation though which a drought event may propagate to climate division *l*. The corresponding Dr_l^{in} indicates the mean geographical distance from which drought may propagate to location *l* along the orientation Or_l^{out}. We formulated these two metrics to include the direction and weight aspects of a network. However, the metrics with similar names but different interpretations were introduced in Rheinwalt et al. (2016) and Boers et al. (2014a,b) for the case of undirected-unweighted networks.

4. Results and discussions

4.1. Effect of thresholds on general characteristics of drought events (1900–2016)

By utilizing the theory of runs, the estimated number of drought events with a threshold equivalent to PDSI < −1 and duration ≥3 months (i.e. threshold (1): initiation of mild drought) for CONUS is shown in (Fig. 7a). By using this threshold, more number of drought events can be observed in the northwestern, north eastern and southeastern parts of USA. Whereas, the regions located in central part of CONUS has relatively less number of drought events. We calculated the duration of mild onset drought as the number of months with PDSI values continuously below the value of −1. Then the average duration of drought per event is determined as the mean of duration of all drought events estimated using the mild onset threshold. The average duration of drought per event (Fig. 7b) is higher in central and southwestern parts in comparison to other regions of CONUS. This indicates that, the drought events classified using this threshold is relatively short, but more frequent in northwestern, northeastern and southeastern parts of CONUS. Whereas, the events in central and southwestern CONUS are relatively longer, but are less frequent. Drought severity is estimated as cumulative sum of PDSI values continuously below the value of −1. Then, the average severity per drought event is estimated as mean of drought severity of all drought events. Similarly, the average intensity per event is calculated as the average of severity divided by duration of its corresponding drought event. Both severity (Fig. 7c) as well as intensity (Fig. 7d) exhibit similar spatial characteristics of higher magnitude in western and central part of CONUS in comparison to eastern part of CONUS. Overall, it was observed that these characteristics vary spatially across continental CONUS in accordance with previous studies (Anderson et al., 2011; Andreadis et al., 2005).

The number of drought events with a threshold equivalent to PDSI < −2 and duration ≥3 months (i.e. threshold (2): initiation of moderate drought) across CONUS is shown in Fig. 8(a). We estimate average duration of drought, average severity per event and average intensity per drought event similar to the case of mild drought onset but with a threshold of −2. More number of drought events can be observed in the southern and western parts of USA.

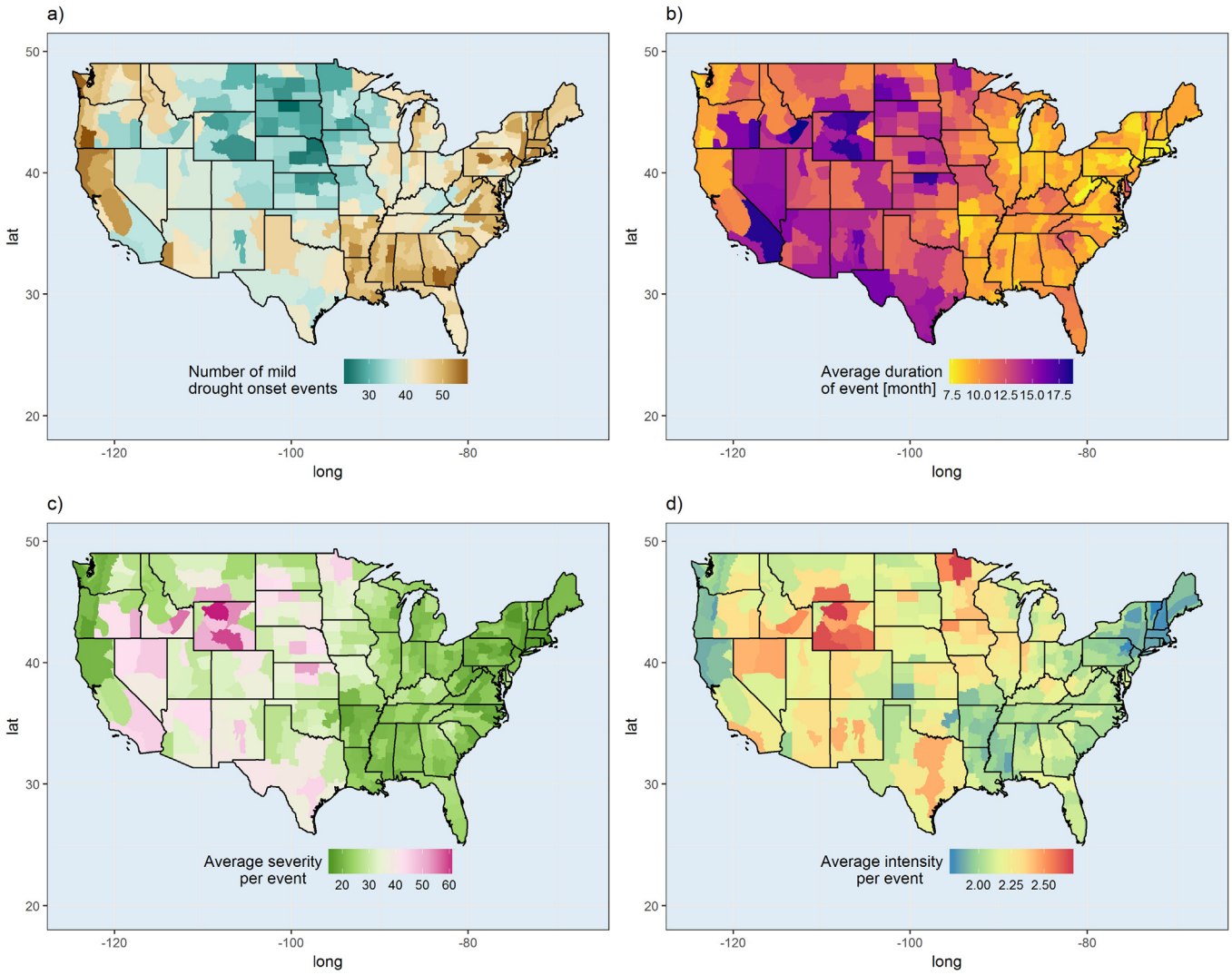

Fig. 7. Spatial distribution of (a) number of mild drought onset events, (b) average duration of drought in months when considering the mild drought onset, (c) average severity per event, and (d) Average intensity per event.

Whereas, the central and eastern CONUS region have relatively less number of drought events. The average duration of drought events (Fig. 8(b)) is higher in central and southwestern CONUS regions. Therefore, droughts in southwestern regions are both frequent and considerably longer duration. However, the drought events in central part of CONUS are relatively short, but more frequent. In the eastern part of CONUS, droughts are less frequent as well as comparatively shorter in duration. In terms of severity (Fig. 8c) and intensity (Fig. 8d), the central north part of CONUS witness higher magnitude compared to other regions. In addition, the drought characteristics varies spatially across continental CONUS similar to previous studies (Ganguli and Ganguly, 2016; Ge et al., 2016).

In summary, the spatial patterns of droughts vary significantly with respect to thresholds. As the threshold is low for initiating mild drought events, it leads to more number of drought events as well as longer drought duration (Fig. 7b). However, increasing the threshold to initiate a moderate drought event led to higher drought severity (intensity) in comparison to mild drought events. Therefore, by studying networks using different drought thresholds can provide insights on drought propagation properties at different severity levels.

4.2. Propagation of drought and their associated strength

The spatial patterns of outward-strength derived based on mild and moderate drought onset networks are shown in Fig. 9. In case of mild drought onset, higher magnitude of outward-strength are concentrated around the Ohio River valley region of USA and lower values occur in all the other regions of USA (Fig. 9a). Higher outward-strength in case of mild drought onset network (i.e., threshold 1) emerges from the central east part of CONUS region or more particularly known as Ohio Valley region. As a result, climate divisions in that region may have a potential influence in early drought propagation to other regions. In addition, in the case of moderate drought onset, Ohio River Valley region has higher values of outward-strength compared to other regions of USA (Fig. 9b). Higher outward-strength in case of moderate drought onset indicates that these regions may likely to play an important role in propagation of droughts to other regions at a later stage. Therefore, if drought onsets in any of the higher outward-strength regions, it is more likely that it would propagate to other divisions creating a regional drought with large spatial extent. However, the geographical area of higher outward-strength divisions in case of mild onset is comparatively more than that of

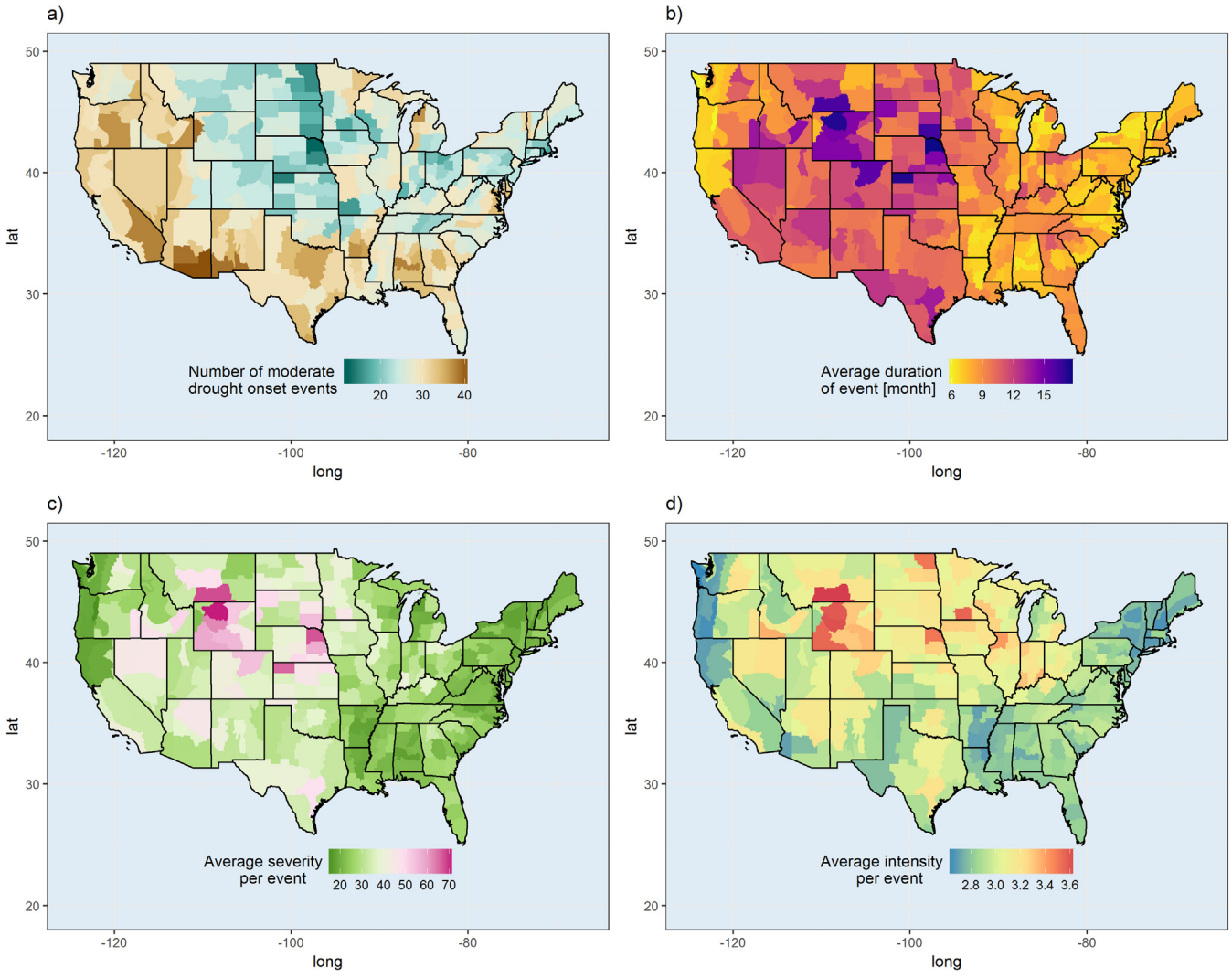

Fig. 8. Spatial distribution of (a) number of moderate drought onset events, (b) average duration of drought in months when considering the moderate drought onset, (c) average severity per event, and (d) average intensity per event.

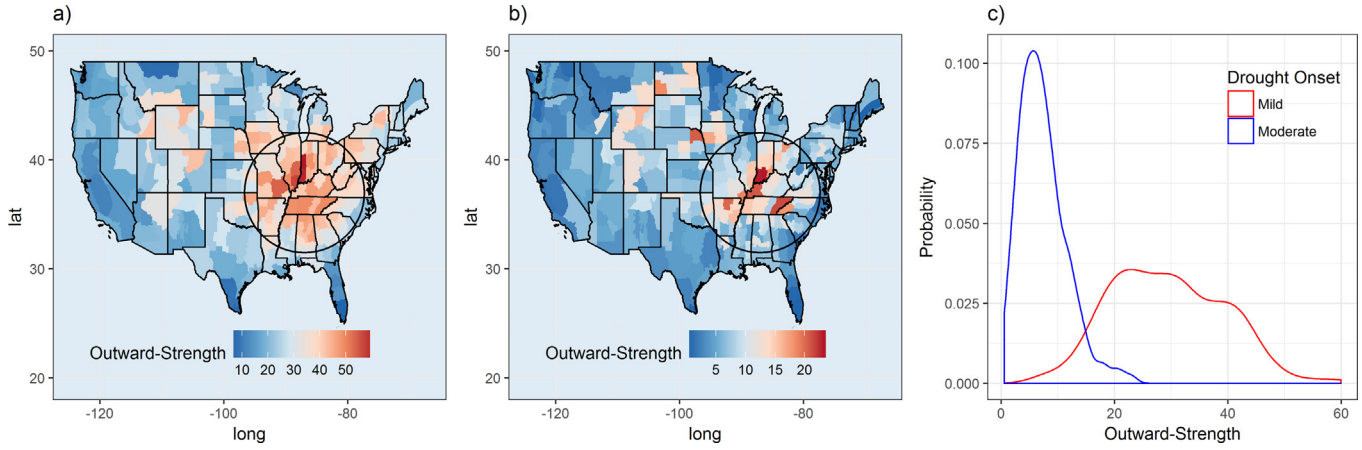

Fig. 9. Spatial distribution of outward-strength in case of (a) mild, and (b) moderate drought onset events, and (c) represents the KS density estimated probability distribution of outward-strength in case of mild and moderate onset of droughts. The region inside the overlaid circle is to highlight the Ohio river valley region.

moderate drought onset. Ohio River Valley seems to be a critical region in this aspect as it plays a role in influencing propagation of mild as well as moderate droughts. This region also known to exhibit highest regional winter moisture variability in the United States, as it is represented by the leading rotated principal component of winter precipitation (Walsh et al., 1982) and the

third principal component of Palmer drought severity index values (Karl and Koscielny, 1982). The leading principal component in the case of winter rainfall indicates that this region contributes significantly to variability of winter precipitation across continental USA. Similarly, the third principal components of the PDSI values indicate substantial variability of drought in that region. Therefore, this change in variability may have contributed to high outward strength values in Ohio River valley. Further, it was observed that the occurrence of an El Nino condition would decrease the precipitation in that region (Zhang et al., 2010). In addition, it was observed that ENSO has a considerable influence on the intra-seasonal temperature extremes in this region (Gershunov and Barnett, 1998). However, it did not appear to be a significant relationship between atmospheric conditions of Ohio River valley with Pacific North American (PNA) index and North Atlantic Oscillation (NAO). As a result, the higher value of out-strength in Ohio River valley may be connected to higher climate variability as well as its teleconnections with ENSO variability.

The kernel density estimates of probability distribution of outward-strength for both mild and moderate drought onset networks are displayed in Fig. 9(c). The probability distributions of outward-strength in both scenarios are significantly different from each other. In case of mild drought onset, distribution is regular and more extensive indicating the outward-strength is higher and it has more spatial variability. Also, the shape of probability distribution in case of a mild drought onset network can be said to have characteristics of a random network due to its modality (Barabasi and Albert, 1999). Whereas, the distribution of moderate drought onset event's outward-strength is a combination of a real and random network (Boccaletti et al., 2006) with majority of the divisions having low values of outward-strength.

Higher values of mild drought onset's inward-strength are observed in northeast, upper Midwest and in parts of southeastern region of CONUS (Fig. 10a). We suggest that higher inward-strength emerges mainly because the climate divisions in that region seems to be influenced even by mild droughts occurring

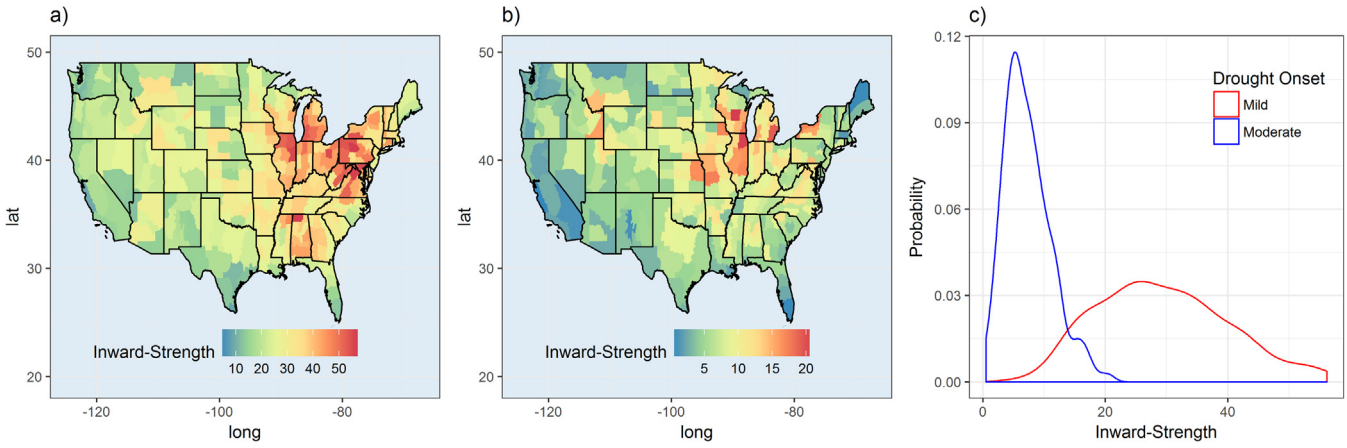

Fig. 10. Spatial distribution of inward-strength in case of (a) mild, and (b) moderate drought onset events, and (c) represents the KS density estimated probability distribution of inward-strength in case of mild and moderate onset of droughts.

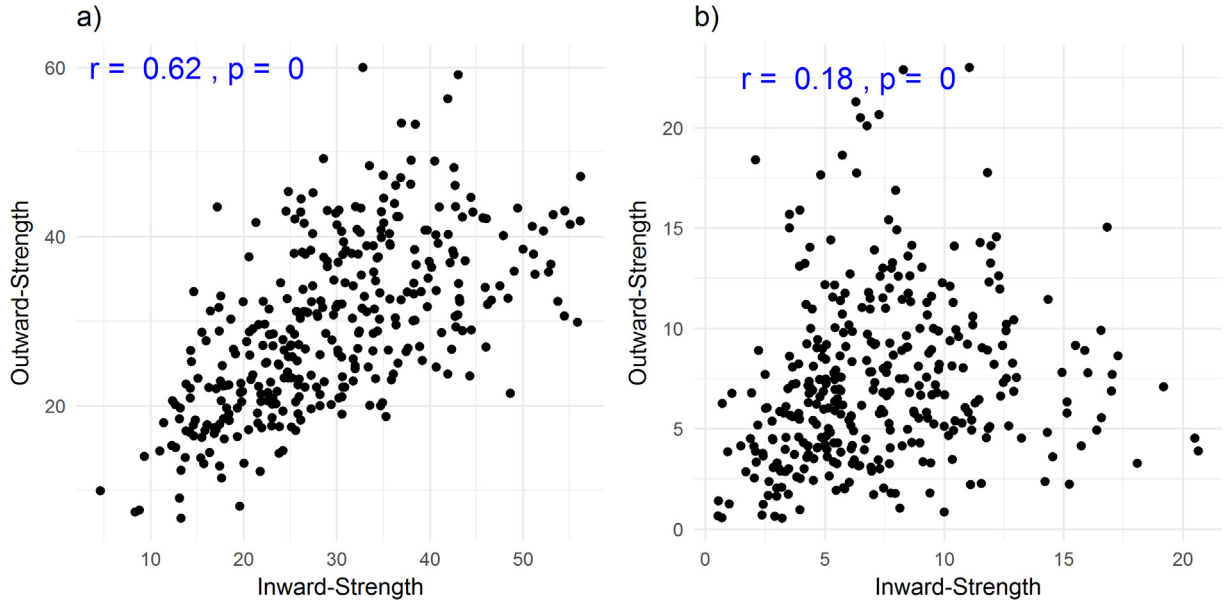

Fig. 11. Scatter plots showing the relation between outward-strength and inward-strength in case of (a) mild, and (b) moderate drought onset events. The Pearson correlation coefficient and its corresponding p value is also shown in blue colored text. (For interpretation of the references to colour in this figure legend, the reader is referred to the web version of this article.)

in other regions and potentially it may have geographically more distant spatial connections. In case of moderate drought onset, only the upper Midwest region has higher values of inward-strength compared to other regions of USA (Fig. 10b). Regions with higher inward-strength are likely to be more influenced by droughts in other regions and are thus more vulnerable. Therefore, these regions might be more sensitive to local climate conditions as well as synoptic climate activity (Mo, 2008; McCabe et al., 2004). The probability distributions of inward-strength in case of both the scenarios (Fig. 10c) have the similar characteristics as in the case of outward-strength (Fig. 9c).

We also analyzed the relation between outward-strength and inward-strength for mild drought onset (Fig. 11a) and moderate drought onset (Fig. 11b) events separately. In case of mild drought onset, a strong linear relationship quantified by high Pearson correlation (r) of 0.62 exists between the outward-strength and inward-strength. This indicates that the climate divisions that influence the drought propagation at an early stage are also vulnerable to early stage droughts propagated from other regions. As a result, it might be difficult to segregate spatial roles of drought propagation at such an early stage. This might explain why it is difficult to detect droughts at an early stage (Mishra and Singh, 2010). However, in case of moderate drought, a weak linear relationship (r = 0.18) exists between outward- and inward-strength. This indicates that the influence and vulnerable regions might not be the same resulting in spatially distinct sink and source regions for drought propagation. Presence of these hotspot regions might help in understanding the dynamics of how drought may propagate at a moderate stage in those regions. Research in similar direction with respect to extreme rainfall events revealed several important characteristics about propagation of extreme events from Southeastern South America to central Andes in South America (Boers et al., 2015a,b; Marwan and Kurths, 2015).

4.3. Orientation characteristics of drought propagation

The outward-orientation for onset of mild and moderate drought events is illustrated in Fig. 12(a) and (b) respectively. Here, Or_l^{out} represents the dominant orientation in which drought at climate division l may propagate to other regions. The number of climate divisions that are likely to propagate droughts in a particular direction are also shown in Fig. 12(c). It can be observed that for most of the climate divisions located in southern part of CONUS, mild drought propagates towards north-northeast (NNE) direction. Similarly, majority of the climate divisions in northeastern CONUS have mild droughts propagating towards the south- southwest (SSW) direction. In addition, mild droughts from few regions located in northern CONUS propagate in the southwestern direction. Interior regions located in northern part of CONUS propagate mild droughts to southern southeast direction. In case of moderate droughts, the orientation pattern seems to be more scattered in

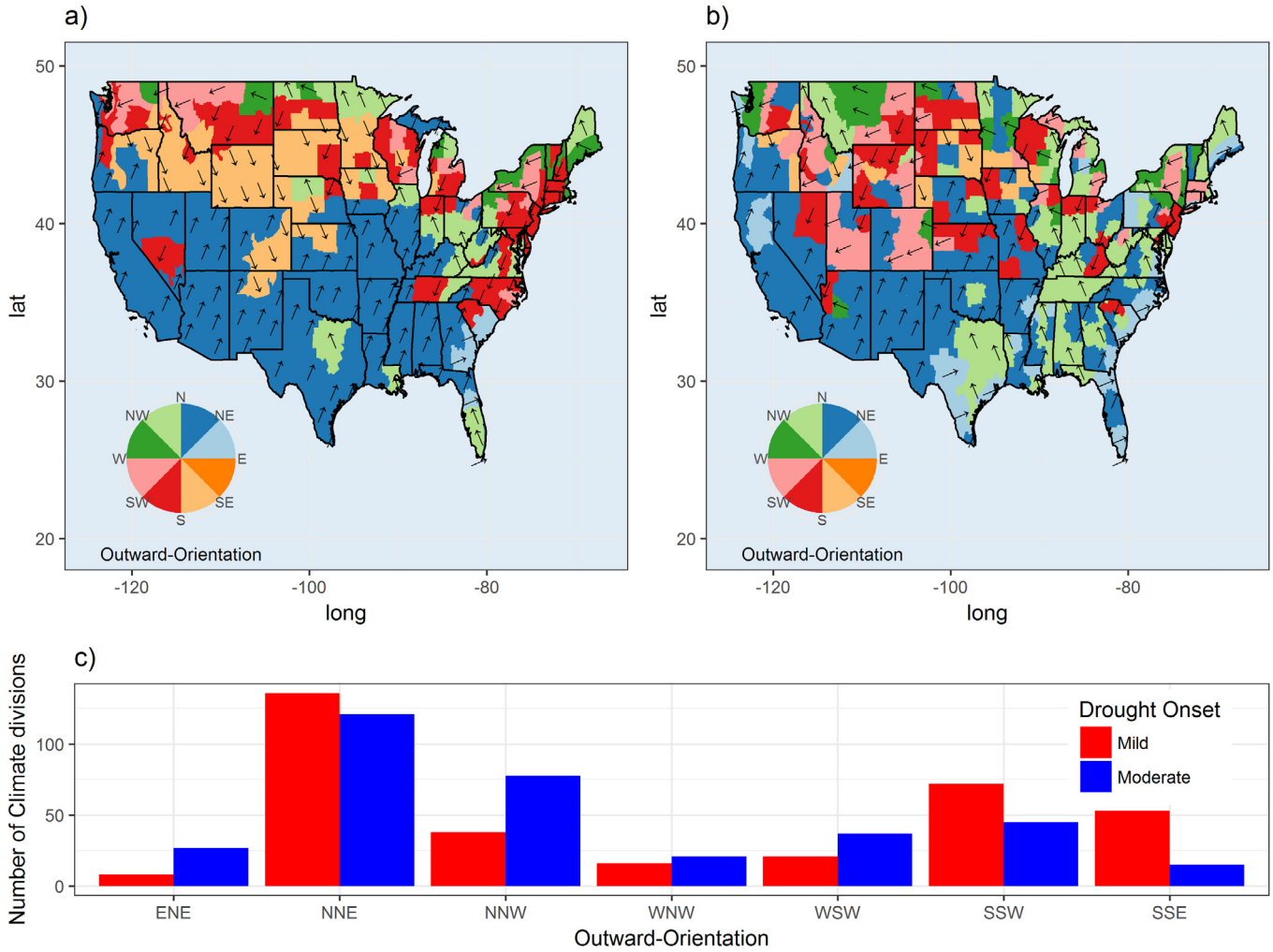

Fig. 12. Spatial distribution of outward-orientation in case of (a) mild, and (b) moderate drought onset events, and (c) represents the number of climate divisions with the corresponding outward-orientations. The arrows on the map indicate direction.

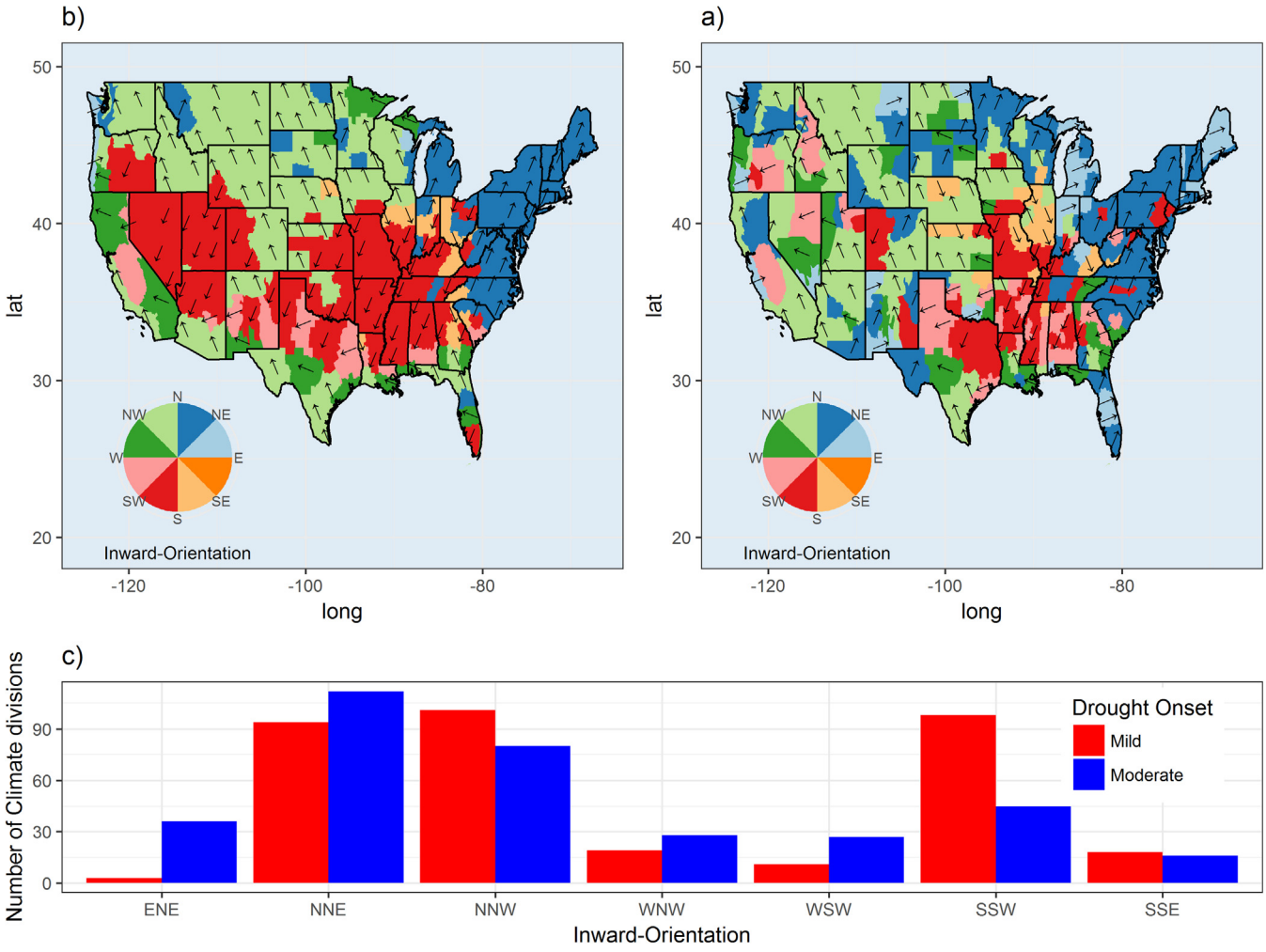

Fig. 13. Spatial distribution of in-orientation in case of (a) mild, and (b) moderate drought onset events. Whereas, (c) represents the number of climate divisions with the corresponding inward-orientations. The arrows on the map indicate direction.

comparison to the case of mild drought (Fig. 12(b)). The areal extents of the orientations are comparatively not as uniform as the latter. The propagation of droughts to the north-northeast (NNE) direction is restricted to only climate divisions of south west. Whereas, comparatively an initiation of moderate droughts in large section of eastern USA likely to propagate in the west-northwest (WNW) direction. Finally, the regions located in north central part of CONUS do not exhibit a uniform orientation as opposed to mild drought events. Overall, our results highlight the orientations for the onsets of mild and moderate droughts, which

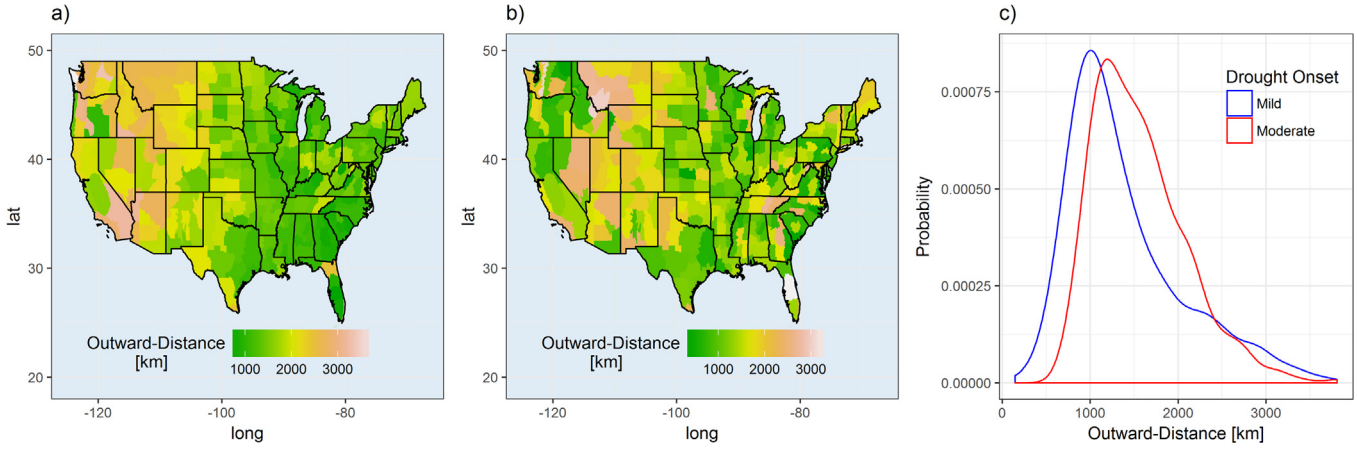

Fig. 14. Spatial distribution of outward-distance in case of (a) mild, and (b) moderate drought onset events, and (c) represents the KS density estimated probability distribution of outward-distance in case of mild and moderate onset of droughts.

have considerable dissimilarity highlighting key fundamental propagation directions spatially.

The inward-orientation for onset of mild and moderate drought events is illustrated in Fig. 13(a) and (b) respectively. Fig. 13(c) provides the number of climate divisions that experience mild and moderate droughts propagating through a particular direction. The peripheral regions from northwest to the southeast of CONUS might experience majority of its mild droughts due to propagation from the northwestern direction. However, the interior Southern CONUS region witness mild droughts propagating from south-southwest (SSW) direction. The northeastern USA usually experiences mild droughts due to propagation from north-northwest (NNW) direction. Similar to the outward-orientation in the case of moderate droughts, the spatial extent of the moderate droughts in case of inward-orientations is also smaller and diverse. The incidence of moderate droughts in majority locations of southwestern USA may originate from the south-southwest (SSW) direction. However, the likelihood of moderate drought for northeastern USA may be originating from the north-northeast (NNE) direction. In the western and most of the central part of USA, they are incidents from northwestern direction. This kind of drought orientation analysis might improve our understanding by illustrating the different aspects of directions of drought propagation. For example, the knowledge of dominant inward and outward orientation of drought propagation might play a key role in developing early warning systems for droughts. For example, if drought occurs in a climate division whose dominant direction outward-orientation is known, and then droughts can be expected in the areas lying in its dominant outward orientation. Similar information can be obtained with the knowledge of inward orientation of a climatic division too.

4.4. Distance characteristics of drought propagation

The spatial distribution of outward-distance in case of mild and moderate drought onset events is shown in Fig. 14(a) and (b) respectively. In case of mild drought events, a clear pattern of shorter propagation distance (<2000 km) can be observed in the

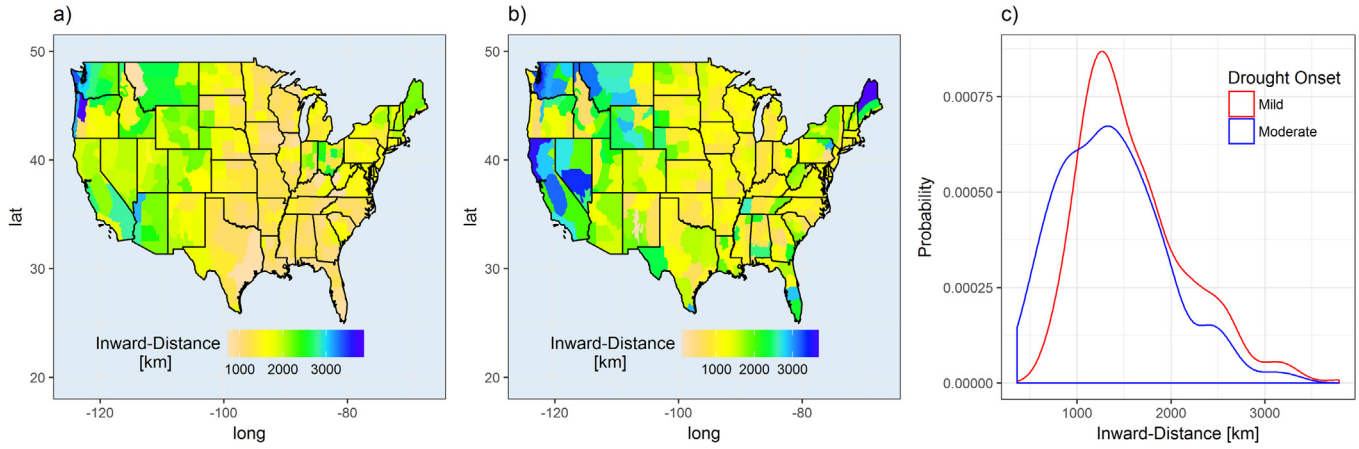

Fig. 15. Spatial distribution of inward-distance in case of (a) mild, and (b) moderate drought onset events, and (c) represents the KS density estimated probability distribution of inward-distance in case of mild and moderate onset of droughts.

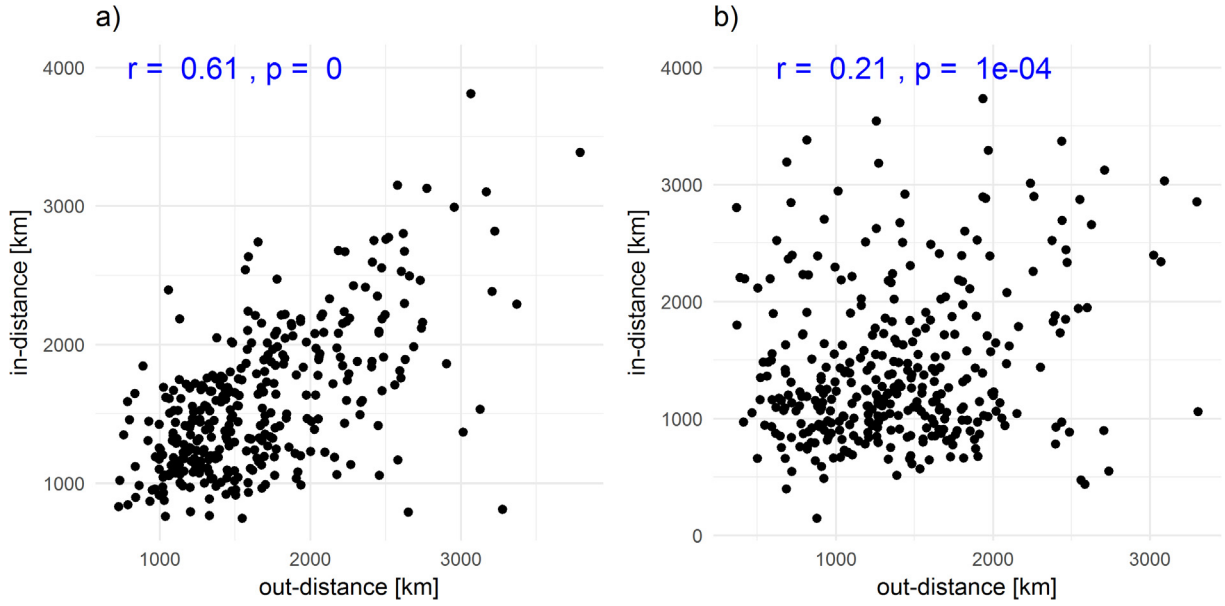

Fig. 16. Scatter plots showing the relation between outward-distance and inward-distance in case of (a) mild, and (b) moderate drought onset events. The Pearson correlation coefficient and its corresponding p value is also shown in blue colored text.

eastern half of USA. Whereas, comparatively longer propagation distances (>2000 km) can be seen in western half of USA. In case of moderate drought, a similar pattern with few exceptions in the Colorado and California regions, where less propagation distances can be observed. Whereas climate divisions located in Georgia and Tennessee and parts of northeastern CONUS exhibit long distance propagation. This spatial pattern closely resembles the spatial map of rainfall entropy of USA (Brunsell, 2010; Martino et al., 2012) indicating that the outward-distance metric might be influenced by rainfall variability. In addition, it is interesting to see that, the probability distribution of outward-distances in case of mild and moderate droughts do not differ much as in the case of strength metrics (Fig. 14c). As a result, even though the inward-strength of mild droughts is higher than that of moderate droughts, the dominance of spatial influence of these drought events is more or less similar.

The spatial distribution of inward-distance in case of mild and moderate drought events is shown in Fig. 15(a) and (b) respectively. The observed spatial pattern of mild drought inward-distance is similar to mild drought outward-distance. The western part has higher values (>2000 km) of inward-distance compared to the eastern CONUS. In case of moderate droughts, a mixed spatial pattern of high inward-distance magnitude is observed over the CONUS. Higher values of inward-distance are observed in western, parts of northeastern and southeastern CONUS. Similar to the probability distribution of outward-distance, it was observed that the probability distribution of mild and moderate droughts inward-distance are similar to each other.

We also analyzed the relation between outward-distance and inward-distance for onset of mild drought (Fig. 16a) and moderate drought (Fig. 16b) events separately. In case of mild droughts, a significant linear relationship quantified by a Pearson correlation (r) of 0.6 exists between outward-distance and inward-distance. This indicates that the climate divisions that have the ability to propagate mild droughts to longer distances also likely to get influenced by drought events from long distances. Whereas, in case of

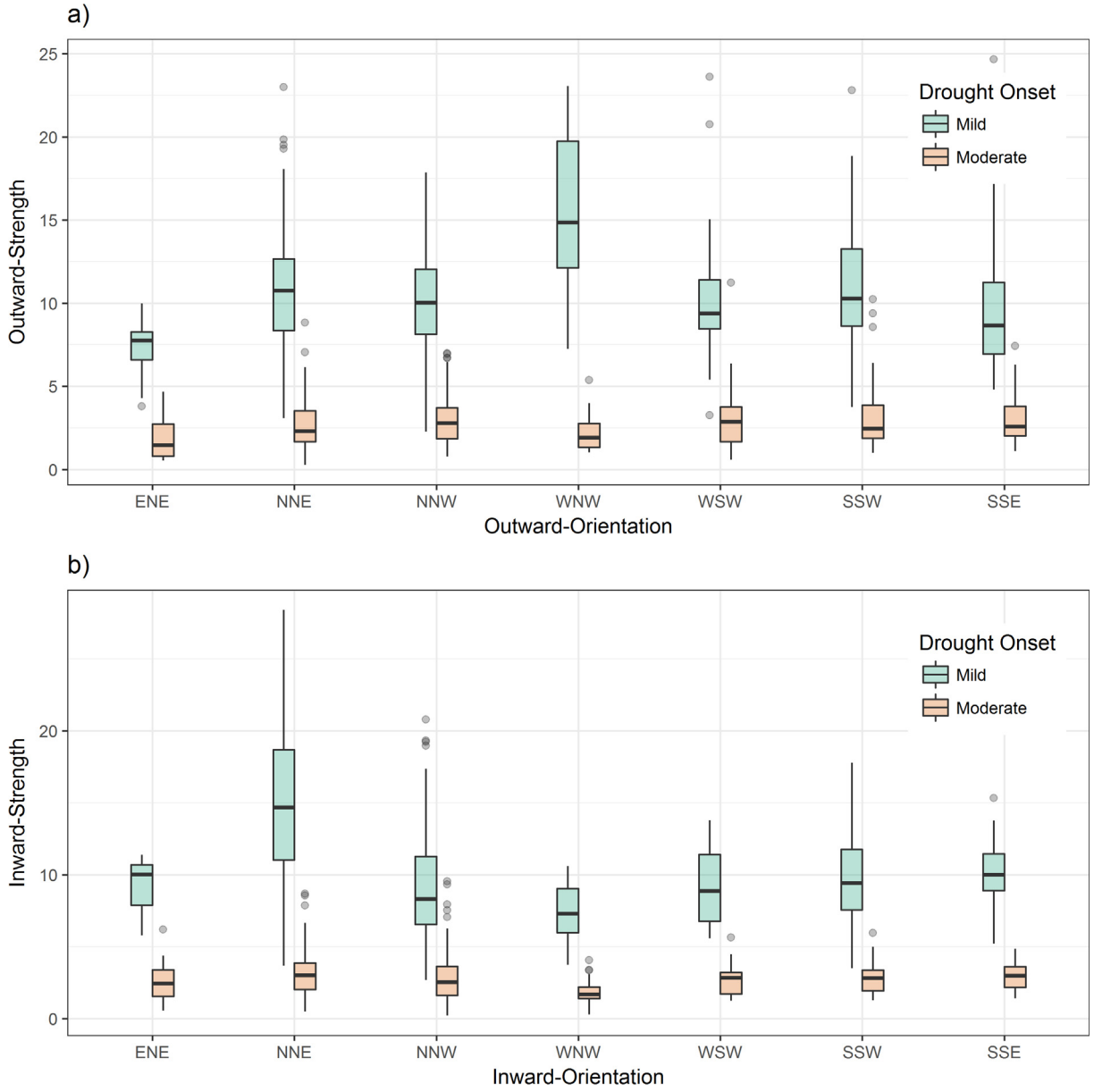

Fig. 17. Box plots showing the variation of (a) outward-strength, and (b) inward-strength along the dominant orientations.

onset of moderate drought events, a weak linear relationship quantified by a Pearson correlation (r) of 0.21 exists between outward-distance and inward-distance. This indicates that the climate divisions that propagate moderate droughts to long distances do not necessarily get influenced by moderate drought events incident from long distances. As a result, different meteorological processes might be controlling the outward- and inward-distances in case of CONUS droughts (Mishra and Singh, 2010; Malik et al., 2012, Stolbova et al., 2014).

4.5. Network characteristics along the dominant directions

In this section, we summarize the variation of the above-discussed network properties of onset of mild and moderate drought events separately along their dominant directions. To illustrate this, we used box plots that summarized the data and its corresponding variation along each direction. We first summarized the outward- and inward-strength against the corresponding outward- and inward-direction in Fig. 17(a) and (b) respectively. The outward-strength values in case of mild drought onset vary across the orientations, and the highest out-strength (median: 15) was observed for west-northwest (WNW) orientation. However, the onset of moderate drought's outward-strengths does not vary across the orientations. Even within the orientations, the outward-strength of mild drought events exhibits considerable variation in comparison to onset of moderate drought events. In the case of inward-strength too, mild drought events vary across the orientations and the highest inward-strength (median: 15) was observed for north-northeast (NNE) orientation.

We summarized inward-distance and outward-distance against the corresponding outward-direction and inward-direction in Fig. 18(a) and (b), respectively. Both outward-distance and inward-distance values are comparable in magnitude and show considerable variations across the orientation unlike the case of strength characteristics. Among the outward-distance values for mild droughts, south-southeast (SSE) and east-northeast (ENE)

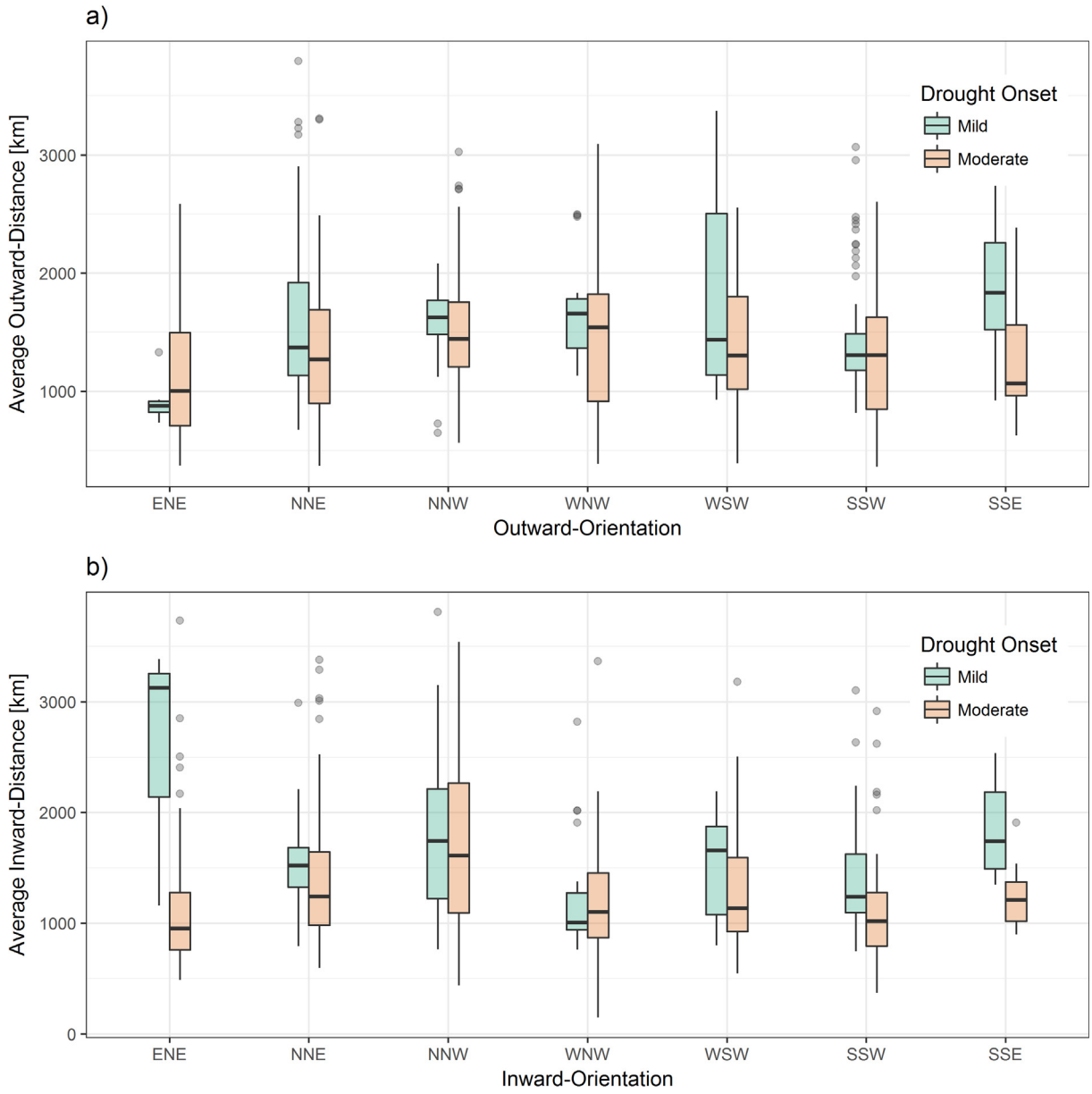

Fig. 18. Box plots showing the variation of (a) average outward-distance, and (b) inward-distance along the dominant orientations.

orientation demonstrated comparatively longer (median: 1800 km) and shorter propagation distances, respectively. Whereas, in the case of moderate droughts, comparatively longer and shorter propagation distances were exhibited along the west-northwest (WNW) and east-northeast (ENE) directions respectively. Contrary to the case of strength characteristics, moderate droughts exhibited higher outward-distance variability within the orientations compared to the mild droughts. The longer inward-distance (median: 3100 km) values for mild drought events was observed along the east-northeast (ENE) direction. Surprisingly, the same direction (ENE) has the shortest inward-distance (median: 1000 km) in case of moderate droughts. This differential behavior highlights the fact that even though mild and moderate droughts are derived from the same index (i.e. PDSI), the controlling factors for these events may be completely different (Lohani et al., 1998; Steinemann, 2003).

5. Summary and conclusions

This study reviews the complex network approaches used for investigating hydroclimatic extreme events. A detailed discussion is provided on complex networks and extreme events, event synchronization method, construction of networks, their statistical significance and the associated network evaluation metrics. In addition to review, we illustrated the application of the complex network theory built upon the event synchronization metric to study the propagation of mild and moderate drought onsets using PDSI monthly time series for a period of 1900–2016. We also introduced two new metrics (orientation and distance) to characterize the spatio-temporal propagation of drought in Continental USA. The following conclusions can be drawn from the application of networks to droughts in this study:

(1) The properties of spatial connections varies when the droughts propagates at different initiation thresholds (i.e., PDSI < −1 and PDSI < −2). Overall, it was observed that the Ohio River valley region may be treated as a dominant region to initiate the drought propagation. Similarly, the upper Midwest section region of CONUS is likely to be vulnerable to spatial propagation of drought events happening elsewhere. As a result, further investigations of atmospheric and hydroclimatic processes in these locations within a network perspective might improve our understanding in identifying appropriate processes responsible for propagation of droughts in CONUS.
(2) It is important to understand that even though the probability distribution of strength characteristics is different, the location of hot spots (i.e. Ohio River Valley and upper Midwestern CONUS) found to be similar at both selected thresholds. However, the strength characteristics for onset of mild drought events are more spatially extensive compared to the onset of moderate drought events. In addition to that, in case of mild drought, a significant linear relationship exists between inward-strength and outward-strength; whereas, a weaker relationship exists between inward-strength and outward-strength for onset of moderate drought.
(3) The orientation of droughts offers a new perspective on understanding the ability of regions to propagate droughts in a particular direction. It was observed that the droughts initiated at a lower threshold (PDSI < −1) can exhibit more clustered and spatially uniform orientations compared to a higher drought thresholds (PDSI < −2).
(4) The distance characteristics shows existence of long distance propagation in the western regions in comparison to the eastern part of CONUS. This kind of information can be beneficial for developing early drought warning systems to improve water management. For example, if drought is already present in a particular climate division, this information can be applied to alert the regions in its dominant outward-orientation and within the propagation distance (outward-distance) ahead of time. Similarly, the inward-distance and inward-direction metrics can also be incorporated in early warning drought systems.
(5) One of the primary purposes of drought investigation is to understand the propagation of spatio-temporal droughts for a given region (Mishra and Singh, 2010). Although we illustrated preliminary results about drought propagation, we still need to build up on this network model to include additional hydro-climatic factors like rainfall, temperature, streamflow to form a set of interacting networks to further understand and predict the drought propagation and occurrence in a space-time dimension. We recognize that the research related to application of network theory in hydrologic and environmental systems are still in its nascent stage and we believe that the present study on the complex networks application on propagation of drought events will advance our understanding on origin and propagation of hydroclimatic extremes.

Acknowledgements

This study was supported by National Science Foundation (NSF) grant # 1653841. Authors would like to thanks NOAA for providing free access to PDSI data sets (http://www7.ncdc.noaa.gov/CDO/CDODivisionalSelect.jsp#). We would like to extend our sincere gratitude to anonymous reviewers and editor for the positive and constructive comments that helped us to improve the article significantly.

References

Adamowski, J.F., 2008. Development of a short-term river flood forecasting method for snowmelt driven floods based on wavelet and cross-wavelet analysis. J. Hydrol. 353 (3), 247–266.
Albert, R., Barabási, A., 2002. Statistical mechanics of complex networks. Rev. Mod. Phys. 74, 47.
Alexander, L.V., Zhang, X., Peterson, T.C., Caesar, J., Gleason, B., Klein Tank, A.M.G., Tagipour, A., 2006. Global observed changes in daily climate extremes of temperature and precipitation. J. Geophys. Res. Atmos. 111 (D5).
Anderson, M.C., Hain, C., Wardlow, B., Pimstein, A., Mecikalski, J.R., Kustas, W.P., 2011. Evaluation of drought indices based on thermal remote sensing of evapotranspiration over the continental United States. J. Clim. 24, 2025–2044.
Andreadis, K.M., Clark, E.A., Wood, A.W., Hamlet, A.F., Lettenmaier, D.P., 2005. Twentieth-century drought in the conterminous United States. J. Hydrometeorol. 6, 985–1001.
Barabasi, A.L., Albert, R., 1999. Emergence of scaling in random networks. Science 286, 509–512.
Basher, R., 2006. Global early warning systems for natural hazards: systematic and people-centred. Philos. Trans. Royal Soc. London A: Math. Phys. Eng. Sci. 364 (1845), 2167–2182.
Beguería, S., 2005. Uncertainties in partial duration series modelling of extremes related to the choice of the threshold value. J. Hydrol. 303 (1), 215–230.
Beniston, M., Stephenson, D.B., Christensen, O.B., Ferro, C.A., Frei, C., Goyette, S., Palutikof, J., 2007. Future extreme events in European climate: an exploration of regional climate model projections. Clim. Change 81 (1), 71–95.
Boccaletti, S., Latora, V., Moreno, Y., Chavez, M., Hwang, D., 2006. Complex networks: structure and dynamics. Phys. Rep. 424, 175–308.
Boers, N., Bookhagen, B., Barbosa, H.M., Marwan, N., Kurths, J., Marengo, J., 2014a. Prediction of extreme floods in the eastern Central Andes based on a complex networks approach. Nat. Commun. 5, 5199.
Boers, N., Bookhagen, B., Marengo, J., Marwan, N., von Storch, J., Kurths, J., 2015a. Extreme rainfall of the South American monsoon system: a dataset comparison using complex networks. J. Clim. 28, 1031–1056.
Boers, N., Bookhagen, B., Marwan, N., Kurths, J., 2016. Spatiotemporal characteristics and synchronization of extreme rainfall in South America with focus on the Andes mountain range. Clim. Dyn. 46 (1–2), 601–617.
Boers, N., Bookhagen, B., Marwan, N., Kurths, J., Marengo, J., 2013. Complex networks identify spatial patterns of extreme rainfall events of the South American Monsoon system. Geophys. Res. Lett. 40, 4386–4392.

Boers, N., Donner, R.V., Bookhagen, B., Kurths, J., 2015b. Complex network analysis helps to identify impacts of the El Niño Southern Oscillation on moisture divergence in South America. Clim. Dyn. 45 (3–4), 619–632.
Boers, N., Rheinwalt, A., Bookhagen, B., Barbosa, H.M., Marwan, N., Marengo, J., et al., 2014b. The South American rainfall dipole: a complex network analysis of extreme events. Geophys. Res. Lett. 41, 7397–7405.
Brunsell, N., 2010. A multiscale information theory approach to assess spatial–temporal variability of daily precipitation. J. Hydrol. 385, 165–172.
Bunde, Armin, Eichner, Jan F., Kantelhardt, Jan W., Havlin, Shlomo, 2005. Long-term memory: a natural mechanism for the clustering of extreme events and anomalous residual times in climate records. Phys. Rev. Lett. 94 (4), 048701.
Davis, R.A., Mikosch, T., 2009. The extremogram: a correlogram for extreme events. Bernoulli 15 (4), 977–1009.
Donges, J.F., Zou, Y., Marwan, N., Kurths, J., 2009a. Complex networks in climate dynamics. Eur. Phys. J. Spec. Top. 174, 157–179.
Donges, J.F., Zou, Y., Marwan, N., Kurths, J., 2009b. The backbone of the climate network. EPL (Europhys. Lett.). 87, 48007.
Ebert-Uphoff, I., Deng, Y., 2012. A new type of climate network based on probabilistic graphical models: results of boreal winter versus summer. Geophys. Res. Lett. 39 (19).
Erdos, P., Rényi, A., 1960. On the evolution of random graphs. Publ. Math. Inst. Hung. Acad. Sci. 5 (1), 17–60.
Fang, K., Sivakumar, B., Woldemeskel, F.M., 2017. Complex networks, community structure, and catchment classification in a large-scale river basin. J. Hydrol. 545, 478–493.
Feldhoff, J.H., Lange, S., Volkholz, J., Donges, J.F., Kurths, J., Gerstengarbe, F.W., 2015. Complex networks for climate model evaluation with application to statistical versus dynamical modeling of South American climate. Clim. Dyn. 44 (5–6), 1567–1581.
Ganguli, P., Ganguly, A.R., 2016. Space-time trends in US meteorological droughts. J. Hydrol.: Reg. Stud. 8, 235–259.
Ge, Y., Apurv, T., Cai, X., 2016. Spatial and temporal patterns of drought in the Continental US during the past century. Geophys. Res. Lett. 43, 6294–6303.
Gershunov, A., Barnett, T.P., 1998. Interdecadal modulation of ENSO teleconnections. Bull. Am. Meteorol. Soc. 79 (12), 2715–2725.
Gozolchiani, A., Havlin, S., Yamasaki, K., 2011. Emergence of El Niño as an autonomous component in the climate network. Phys. Rev. Lett. 107, 148501.
Granger, C.W.J., 1969. Investigating causal relations by econometric models and cross-spectral methods. Econometrica 37 (3), 424–438. https://doi.org/10.2307/1912791.
Groisman, P.Y., Knight, R.W., Karl, T.R., 2001. Heavy precipitation and high streamflow in the contiguous United States: trends in the twentieth century. Bull. Am. Meteorol. Soc. 82 (2), 219–246.
Gudendorf, G., Segers, J., 2010. Extreme-value copulas. Copula Theory Appl., 127–145
Halverson, M.J., Fleming, S.W., 2015. Complex network theory, streamflow, and hydrometric monitoring system design. Hydrol. Earth Syst. Sci 19, 3301–3318.
Hamed, K., Rao, A.R. (Eds.), 1999. Flood Frequency Analysis. CRC Press.
Hannaford, J., Lloyd-Hughes, B., Keef, C., Parry, S., Prudhomme, C., 2011. Examining the large-scale spatial coherence of European drought using regional indicators of precipitation and streamflow deficit. Hydrol. Process. 25, 1146–1162.
Hao, Z., AghaKouchak, A., Phillips, T.J., 2013. Changes in concurrent monthly precipitation and temperature extremes. Environ. Res. Lett. 8 (3), 034014.
Hlinka, J., Hartman, D., Vejmelka, M., Novotná, D., Paluš, M., 2014. Non-linear dependence and teleconnections in climate data: sources, relevance, nonstationarity. Clim. Dyn. 42 (7–8), 1873–1886.
Hoskins, B.J., Ambrizzi, T., 1993. Rossby wave propagation on a realistic longitudinally varying flow. J. Atmos. Sci. 50 (12), 1661–1671.
Jain, S., Lall, U., 2001. Floods in a changing climate: Does the past represent the future? Water Resour. Res. 37 (12), 3193–3205.
Jha, S.K., Zhao, H., Woldemeskel, F.M., Sivakumar, B., 2015. Network theory and spatial rainfall connections: an interpretation. J. Hydrol. 527, 13–19.
Kao, S.C., Govindaraju, R.S., 2010. A copula-based joint deficit index for droughts. J. Hydrol. 380 (1), 121–134.
Karl, T.R., Koscielny, A.J., 1982. Drought in the united states: 1895–1981. Int. J. Climatol. 2, 313–329.
Karl, T.R., Riebsame, W.E., 1984. The identification of 10-to 20-year temperature and precipitation fluctuations in the contiguous United States. J. Clim. Appl. Meteorol. 23, 950–966.
Karl, T.R., Williams Jr, C.N., Young, P.J., Wendland, W.M., 1986. A model to estimate the time of observation bias associated with monthly mean maximum, minimum and mean temperatures for the United States. J. Clim. Appl. Meteorol. 25, 145–160.
Kharin, V.V., Zwiers, F.W., Zhang, X., Hegerl, G.C., 2007. Changes in temperature and precipitation extremes in the IPCC ensemble of global coupled model simulations. J. Clim. 20 (8), 1419–1444.
Kim, T.W., Valdés, J.B., 2003. Nonlinear model for drought forecasting based on a conjunction of wavelet transforms and neural networks. J. Hydrol. Eng. 8 (6), 319–328.
Kuczera, G., 1999. Comprehensive at-site flood frequency analysis using Monte Carlo Bayesian inference. Water Resour. Res. 35 (5), 1551–1557.
Kwon, H.H., Lall, U., Kim, S.J., 2016. The unusual 2013–2015 drought in South Korea in the context of a multicentury precipitation record: Inferences from a nonstationary, multivariate Bayesian copula model. Geophys. Res. Lett. 43 (16), 8534–8544.
Leonard, M., Westra, S., Phatak, A., Lambert, M., van den Hurk, B., McInnes, K., Stafford-Smith, M., 2014. A compound event framework for understanding extreme impacts. Wiley Interdiscip. Rev. Clim. Change 5 (1), 113–128.
Lloyd-Hughes, B., 2012. A spatio-temporal structure-based approach to drought characterisation. Int. J. Climatol. 32, 406–418.
Lohani, V., Loganathan, G., Mostaghimi, S., 1998. Long-term analysis and short-term forecasting of dry spells by palmer drought severity index. Hydrol. Res. 29, 21–40.
Madadgar, S., Moradkhani, H., 2013. A Bayesian framework for probabilistic seasonal drought forecasting. J. Hydrometeorol. 14 (6), 1685–1705.
Malik, N., Bookhagen, B., Marwan, N., Kurths, J., 2012. Analysis of spatial and temporal extreme monsoonal rainfall over South Asia using complex networks. Clim. Dyn. 39, 971–987.
Marengo, J.A., Liebmann, B., Grimm, A.M., Misra, V., Silva Dias, P.L., Cavalcanti, I.F.A., Saulo, A.C., 2012. Recent developments on the South American monsoon system. Int. J. of Climatol. 32 (1), 1–21.
Martino, G.D., Fontana, N., Marini, G., Singh, V.P., 2012. Variability and trend in seasonal precipitation in the continental United States. J. Hydrol. Eng. 18, 630–640.
Marwan, N., Kurths, J., 2015. Complex network based techniques to identify extreme events and (sudden) transitions in spatio-temporal systems. Chaos: an Interdisciplinary. J. Nonlinear Sci. 25 (9), 097609.
McCabe, G.J., Palecki, M.A., Betancourt, J.L., 2004. Pacific and Atlantic Ocean influences on multidecadal drought frequency in the United States. Proc. Natl. Acad. Sci. U.S.A. 101, 4136–4141.
McKee, T.B., Doesken, N.J., Kleist, J., 1993. The relationship of drought frequency and duration to time scales. In: Proceedings of the 8th Conference on Applied Climatology. American Meteorological Society, Boston, MA,, pp. 179–183.
Mishra, A.K., Singh, V.P., 2009. Analysis of drought severity-area-frequency curves using a general circulation model and scenario uncertainty. J. Geophys. Res.: Atmos. 114 (D6).
Mishra, A.K., Singh, V.P., 2010. A review of drought concepts. J. Hydrol. 391, 202–216.
Mishra, A.K., Singh, V.P., 2011. Drought modeling–A review. J. Hydrol. 403, 157–175.
Mishra, A.K., Singh, V.P., 2012. Simulating hydrological drought properties at different spatial units in the United States based on wavelet-bayesian regression approach. Earth Interact. 16 (17), 1–23.
Mishra, A.K., Ines, A.V., Das, N.N., Khedun, C.P., Singh, V.P., Sivakumar, B., Hansen, J. W., 2015. Anatomy of a local-scale drought: application of assimilated remote sensing products, crop model, and statistical methods to an agricultural drought study. J. Hydrol. 526, 15–29.
Mo, K.C., 2008. Model-based drought indices over the United States. J. Hydrometeorol. 9, 1212–1230.
Mokhov, I.I., Smirnov, D.A., Nakonechny, P.I., Kozlenko, S.S., Seleznev, E.P., Kurths, J., 2011. Alternating mutual influence of El-Niño/Southern oscillation and Indian monsoon. Geophys. Res. Lett. 38 (8).
Naufan, I., Sivakumar, B., Woldemeskel, F.M., Raghavan, S.V., Vu, M.T., Liong, S., 2017. Spatial connections in regional climate model rainfall outputs at different temporal scales: application of network theory. J. Hydrol.
NOAA National Centers for Environmental Information (NCEI) U.S. Billion-Dollar Weather and Climate Disasters (2017). https://www.ncdc.noaa.gov/billions/ (Retrived on 29th July, 2017).
Özger, M., Mishra, A.K., Singh, V.P., 2009. Low frequency drought variability associated with climate indices. J. Hydrol.. 364, 152–162.
Portela, M.M., dos Santos, J.F., Silva, A.T., Benitez, J.B., Frank, C., Reichert, J.M., 2015. Drought analysis in southern Paraguay, Brazil and northern Argentina: regionalization, occurrence rate and rainfall thresholds. Hydrol. Res. 46 (5), 792–810.
Puccetti, G., Wang, R., 2015. Detecting complete and joint mixability. J. Comput. Appl. Math. 280, 174–187.
Quiroga, R.Q., Kreuz, T., Grassberger, P., 2002. Event synchronization: a simple and fast method to measure synchronicity and time delay patterns. Phys. Rev. E 66, 041904.
Rajsekhar, D., Mishra, A.K., Singh, V.P., 2012. Regionalization of drought characteristics using an entropy approach. J. Hydrol. Eng. 18 (7), 870–887.
Rajsekhar, D., Singh, V.P., Mishra, A.K., 2015. Multivariate drought index: an information theory based approach for integrated drought assessment. J. Hydrol. 526, 164–182.
Rheinwalt, A., Boers, N., Marwan, N., Kurths, J., Hoffmann, P., Gerstengarbe, F., et al., 2016. Non-linear time series analysis of precipitation events using regional climate networks for Germany. Clim. Dyn. 46, 1065–1074.
Romatschke, U., Houze Jr, R.A., 2010. Extreme summer convection in South America. J. Clim. 23 (14), 3761–3791.
Runge, J., Petoukhov, V., Donges, J.F., Hlinka, J., Jajcay, N., Vejmelka, M., Kurths, J., 2015. Identifying causal gateways and mediators in complex spatio-temporal systems. Nat. commun. 6, 8502.
Salio, P., Nicolini, M., Zipser, E.J., 2007. Mesoscale convective systems over southeastern South America and their relationship with the South American low-level jet. Monthly Weather Rev. 135 (4), 1290–1309.
Samaniego, L., Bárdossy, A., Kumar, R., 2010. Streamflow prediction in ungauged catchments using copula-based dissimilarity measures. Water Resour. Res. 46 (2).
Scarsoglio, S., Laio, F., Ridolfi, L., 2013. Climate dynamics: a network-based approach for the analysis of global precipitation. PLoS One 8, e71129.
Schreiber, T., 2000. Measuring information transfer. Phys. Rev. letters 85 (2), 461.

Sheffield, J., Andreadis, K.M., Wood, E.F., Lettenmaier, D.P., 2009. Global and continental drought in the second half of the twentieth century: severity–area–duration analysis and temporal variability of large-scale events. J. Clim. 22, 1962–1981.
Sillmann, J., Kharin, V.V., Zhang, X., Zwiers, F.W., Bronaugh, D., 2013. Climate extremes indices in the CMIP5 multimodel ensemble: Part 1. Model evaluation in the present climate. J. Geophys. Res.: Atmos. 118 (4), 1716–1733.
Sivakumar, B., Woldemeskel, F.M., 2015. A network-based analysis of spatial rainfall connections. Environ. Modell. Software 69, 55–62.
Sivakumar, B., Woldemeskel, F., 2014. Complex networks for streamflow dynamics. Hydrol. Earth Syst. Sci. 18, 4565.
Sivapalan, M., 2003. Prediction in ungauged basins: a grand challenge for theoretical hydrology. Hydrol. Processes 17 (15), 3163–3170.
Smakhtin, V.U., 2001. Low flow hydrology: a review. J. Hydrol. 240 (3), 147–186.
Song, S., Singh, V.P., 2010. Meta-elliptical copulas for drought frequency analysis of periodic hydrologic data. Stochastic Environ. Res. Risk Assess. 24 (3), 425–444.
Srinivas, V.V., Tripathi, S., Rao, A.R., Govindaraju, R.S., 2008. Regional flood frequency analysis by combining self-organizing feature map and fuzzy clustering. J. Hydrol. 348 (1), 148–166.
Stahl, K., Demuth, S., 1999. Linking streamflow drought to the occurrence of atmospheric circulation patterns. Hydrol. Sci. J. 44 (3), 467–482.
Steinemann, A., 2003. Drought indicators and triggers: a stochastic approach to evaluation. JAWRA J. Am. Water Resour. Assoc. 39, 1217–1233.
Steinhaeuser, K., Ganguly, A.R., Chawla, N.V., 2012. Multivariate and multiscale dependence in the global climate system revealed through complex networks. Clim. Dyn. 39, 889–895.
Stolbova, V., Martin, P., Bookhagen, B., Marwan, N., Kurths, J., 2014. Topology and seasonal evolution of the network of extreme precipitation over the Indian subcontinent and Sri Lanka. Nonlinear Processes Geophys. 21, 901–917.
Su-Hong, H., Tai-Chen, F., Yan-Chun, G., Yan-Hua, H., Cheng-Guo, W., Zhi-Qiang, G., 2014. Predicting extreme rainfall over eastern Asia by using complex networks. Chinese Phys. B 23 (5), 059202.
Sun, X., Thyer, M., Renard, B., Lang, M., 2014. A general regional frequency analysis framework for quantifying local-scale climate effects: a case study of ENSO effects on Southeast Queensland rainfall. J. Hydrol. 512, 53–68.
Thibaud, E., Mutzner, R., Davison, A.C., 2013. Threshold modeling of extreme spatial rainfall. Water Resour. Res. 49 (8), 4633–4644.
Tsonis, A.A., Roebber, P.J., 2004. The architecture of the climate network. Phys. A: Stat. Mech. Appl. 333, 497–504.
Tsonis, A.A., Swanson, K.L., Roebber, P.J., 2006. What do networks have to do with climate? Bull. Am. Meteorol. Soc. 87, 585–595.
Van Loon, A.F., 2015. Hydrological drought explained. Wiley Interdiscip. Rev.: Water 2, 359–392.
Vera, C., Higgins, W., Amador, J., Ambrizzi, T., Garreaud, R., Gochis, D., Nogues-Paegle, J., 2006. Toward a unified view of the American monsoon systems. J. Clim. 19 (20), 4977–5000.
Von Storch, H., 1999. Misuses of statistical analysis in climate research pp. 11–26. Analysis of Climate Variability. Springer, Berlin Heidelberg.
Walsh, J.E., Richman, M.B., Allen, D.W., 1982. Spatial coherence of monthly precipitation in the United States. Mon. Weather Rev. 110, 272–286.
Watts, D.J., Strogatz, S.H., 1998. Collective dynamics of small-world networks. Nature 393, 440.
Wright, S., 1921. Correlation and causation. J. Agric. Res. 20 (7), 557–585.
Xu, K., Yang, D., Yang, H., Li, Z., Qin, Y., Shen, Y., 2015. Spatio-temporal variation of drought in China during 1961–2012: a climatic perspective. J. Hydrol. 526, 253–264.
Yang, P., Xiao, Z., Yang, J., Liu, H., 2013. Characteristics of clustering extreme drought events in China during 1961–2010. Acta Meteorol. Sinica 27 (2), 186–198.
Yoo, Jiyoung, Kwon, Hyun-Han, Kim, Tae-Woong, Ahn, Jae-Hyun, 2012. Drought frequency analysis using cluster analysis and bivariate probability distribution. J. Hydrol. 420, 102–111.
Zhan, W., Guan, K., Sheffield, J., Wood, E.F., 2016. Depiction of drought over sub-Saharan Africa using reanalyses precipitation data sets. J. Geophys. Res.: Atmos. 121.
Zhang, X., Wang, J., Zwiers, F.W., Groisman, P.Y., 2010. The influence of large-scale climate variability on winter maximum daily precipitation over North America. J. Clim. 23 (11), 2902–2915.